AN EXPERIMENTAL STUDY OF CAPILLARY WAVEGUIDE TECHNIQUES APPLIED TO NONLINEAR OPTICS

by

Andrew John Berry

Ph.D. November 1983

UNIVERSITY OF SOUTHAMPTON

AN EXPERIMENTAL STUDY OF CAPILLARY WAVEGUIDE TECHNIQUES APPLIED TO NONLINEAR OPTICS

by

Andrew John Berry

A thesis submitted for the degree of

Doctor of Philosophy

Department of Electronics

Faculty of Engineering and Applied Science

November 1983

UNIVERSITY OF SOUTHAMPTON

ABSTRACT

FACULTY OF ENGINEERING AND APPLIED SCIENCE

ELECTRONICS

Doctor of Philosophy

AN EXPERIMENTAL STUDY OF CAPILLARY WAVEGUIDE TECHNIQUES APPLIED TO NONLINEAR OPTICS

by Andrew John Berry

This thesis describes investigations made into the nonlinear optical processes of Stimulated Raman and Brillouin Scattering in simple gases when they are performed in various guided configurations.

In order to make a detailed comparison between experiment and theory a well defined pump beam is required. The development and operation of a laser capable of producing such a beam, the pre-lase Q-switched, Nd:YAG telescopic resonator, is described in the first part of this thesis. The output from this laser, and the harmonics derived from it, were then used to perform simple unguided SRS and SBS experiments to provide results against which the performance of the guided configurations can be compared. This also allowed a check to be made of the accuracy of the theoretical predictions of SRS and SBS in gases, so that we could be confident about extending the theory to the case of guided configurations.

The waveguiding properties of hollow, cylindrical, quartz capillaries are then described, along with the associated problems of coupling radiation into and out of them. Assuming next that a nonlinear medium is contained within the hollow core, theoretical expressions are developed for the SRS and SBS threshold powers for various configurations that include single pass, resonator and oscillator-amplifier systems. In the final part of the thesis these predictions are tested experimentally, in each case good agreement being found. The main conclusion to be made, finally, is that the use of waveguides substantially reduces the threshold powers required for these nonlinear processes.

CONTENTS

1. INTRODUCTION

The widespread activity and progress in the development of tunable coherent light sources in recent years is largely as a result of the possibilities they offer in spectroscopy and chemical analysis. The advances that have been made by these sources stem from their high power, spectral brightness, directionality and, in some cases, their capability for short time-resolution. To date, however, most of the tunable sources that have been developed operate over only a limited range of the spectrum, and in general, the best sources tend to be limited to the visible region. (dye lasers being the obvious example) It is the mid-infrared region (1.5-20μm), however, which is of particular interest to the molecular spectroscopist since it is in this region that many molecules display their most characteristic absorption bands. Tunable sources in this region are therefore a very useful tool in the detection and analysis of molecular species, one example of their use being atmospheric pollution monitoring. Also, they allow the possibility of selective excitation of chemical reactions or selec tive dissociation. A good example of the use of the latter process is provided by the isotope separation by photodissociation of uranium hexafluoride.

Various methods of generating tunable radiation in the 1.5-20μm region have therefore been investigated. Semiconductor diode lasers have been discontinuously tuned over the range 4-30 μm, and generate typically 10mW (cw) and 10W (pulsed) but they usually require low temperature operating conditions and each diode has only a limited tuning range.

Optical Parametric Oscillation in various nonlinear crystals has been used to down-convert fixed frequency laser radiation and produce a tunable source over much of the region and can, indeed, produce powers of tens of kilowatts in a linewidth of about 1 cm^{-1}. Problems here, however, include the small margin between threshold being reached for the process and damage of the crystal.

More recently, however, interest has been shown in techniques where the tunability of a well-established source in the visible, say a dye laser, can be shifted directly into the infrared by various nonlinear scattering interactions. The most convenient method is by Stimulated Raman Scattering (SRS). Interest was focussed in particular on Stimulated Electronic Raman Scattering (SERS) in atomic vapours since the large shifts available (20,000-30,000 cm^{-1}) allowed the typical dye laser tunability to be shifted well into the infrared. Unfortunately, however, serious limitations are imposed by various competing processes. In any case, the heat pipes necessary to maintain the atomic (metal) vapours prove to be somewhat inconvenient. There are, however, two further approaches to the problem, both of which will be considered in the work of this thesis. The first is to again use SRS of the output from visible dye lasers, but this time in the well known simple molecular gases such as H_2, D_2 and CH_4. These gases have Raman Shifts which, although not as large as the $\sim$25,000 cm^{-1} available with atomic metal vapours, are still quite large (e.g. 4155 cm^{-1} for H_2). The mid-infrared region is covered, therefore, not just by the tunable 1st Stokes shifted radiation, but by the multiple stokes shifted components. It is necessary, therefore, that good efficiencies be obtained for conversion to the higher order Stokes components. One method of ensuring this is to perform the SRS process in a waveguide.

The second approach again involves SRS in simple molecular gases, but this time using the tunable output of lasers already operating in the near-infrared region of the spectrum. Such lasers, still only in the development stage, include the so called "vibronic" lasers (e.g. nickel or cobalt doped magnesium fluoride; Alexandrite) and the new colour or F-centre lasers. Between them these lasers have so far been tuned over the range 0.8 - 3.5 μm and so a single shift in, say, H_2 would cover the entire mid-infrared region of the spectrum. The main problem with this approach, however, is expected to be the difficulty in obtaining high enough output powers to reach SRS threshold in the molecular gases, a problem which is aggravated by the unfavourable wavelength dependence of the Raman gain. It is necessary, therefore, to develop various techniques for lowering the threshold powers required, and in particular, we will investigate the capability of waveguide configurations to provide just this effect.

The work in this thesis was directed therefore, towards establishing the performance, limitations and a general assessment of the advantages of performing nonlinear optical interactions, particularly SRS, in waveguide configurations. This work required as perhaps its most important element a well-behaved and well-characterised pump beam. This enables one to make careful comparisons between theory and experiment. The output of a carefully designed Nd:YAG laser and its harmonics were used as the pump beams. Although obviously not tunable, such pump beams should provide the best possible results by which future experiments using tunable sources can be judged. In chapter 2, therefore, the theory and operation of a "telescopic resonator" Nd:YAG laser provides an output beam which is TEM_{oo}, SLM with a smooth Gaussian temporal profile and has a reliable high energy and power (Typically 100mJ in 25ns implying 4MW).

In chapter 3 the general theory of SRS and the often competing process of Stimulated Brillouin Scattering (SBS) is presented, with particular attention being paid to deriving threshold expressions for practical unguided pumping conditions using pump beams of the type derived from the telescopic resonator of chapter 2. Briefly mentioned also are the extensions of this theory to transient conditions and the possible use of an unguided Raman resonator. Chapter 4 describes the experimental test of the theoretical predictions of chapter 3 for the case of single-pass, tightly focussed, unguided SRS and SBS. These measurements were made to provide a benchmark against which the performance of guided wave processes will be judged, but also good agreement was sought between theory and experiment to give confidence both in the values of material parameters used and in the later extension of the theory to handle the guided wave situations. This theory is presented in chapter 5, where first the general properties of hollow dielectric waveguides are described. The guided configurations then considered include single pass SRS and SBS, SRS in waveguide resonators, single pass SRS using short pulses (but still steady-state) and finally SRS using synchronous pumping of a waveguide resonator. All these cases were investigated experimentally as described in chapter 6. Particular interest was shown in the threshold reductions obtained when compared to the unguided results of chapter 4, and the good agreement that is obtained between theory and experiment. This agreement allows successful conclusions to be reported in chapter 7 and also allows confident predictions to be made for future investigations, particularly when using dye lasers as the tunable pump source.

2. THEORY AND OPERATION OF THE TELESCOPIC RESONATOR

In the first part of this chapter the basic theory of the telescopic resonator and pre-lase Q-switching is presented. It will be shown that the output of a laser designed and built using this theory should have the necessary properties to permit an accurate, quantitative study of nonlinear optical processes. This theory is put to the test in the second part of the chapter where the results are presented of the design and operation of telescopic resonators incorporating three different Nd:YAG rod sizes. All three rods were operated fixed-Q, fast Q-switched and pre-lase Q-switched with variable, though theoretically predictable, degrees of success.

2.1 High Power, Low Divergence Operation of Nd:YAG Lasers

The most desirable beam from a laser is the circulary symmetric TEM_{oo} mode. There are a number of reasons for this, perhaps the most important being that such a beam has the diffraction-limited minimum divergence and hence can be used to obtain a maximum intensity per unit solid angle - a quantity of great importance in many applications. The TEM_{oo} mode is also the easiest to handle in an analysis of non-linear interactions. This is particularly true when considering non-linear optics in waveguides since it is the TEM_{oo} mode which couples with 98% efficiency to the lowest order, lowest loss EH_{11} mode of the guide, as we shall see later. Ways must be found, therefore, of ensuring that only a TEM_{oo} mode is allowed to oscillate (since in general a cavity can simultaneously support many modes) and that as much energy as possible is contained within it.

The standard results for the spotsizes of the two end mirrors of an empty resonator are well known (Kogelnic and Li, 1966);

$$\frac{\pi W_{1,2}^2}{\lambda} = L \left[\frac{g_{2,1}}{g_{1,2}(1-g_1 g_2)} \right]^{\frac{1}{2}} \qquad 2.1$$

where;

$$g_{1,2} = 1 - L/R_{1,2} \qquad 2.2$$

For solid-state lasers such as Nd:YAG, however, this empty cavity analysis is insufficient because the rod itself acts as a variable positive lens under typical flashlamp pumping conditions - the focal length depending on flashlamp energy and repetition rate.

Assuming that the rod is near one mirror its focal length can be incorporated into a new effective radius of curvature of that mirror. If this operation is performed and typical rod focal lengths of 5-10m are assumed, then for ~1m long cavities the TEM_{oo} spotsizes predicted by equations 2.1 and 2.2 are rather small and one has no chance of getting a large energy from the rod into a TEM_{oo} output beam.

It has long been appreciated that the rod focal length can be compensated for and hence an arbitrarily large W_2 obtained. Equations 2.1 and 2.2 show that if R_1 is plane, $g_1 = 1$ and then if $g_2 = 1$ (say, by making $R_2 = -f_R$, the focal length of the rod, the rod being assumed close to mirror 2) then W_2 tends to infinity. The problem with this approach is that W_2 is then very sensitive to slight variations in g_2 caused by, amongst other things, shot to shot variatons in flashlamp pulse energy and hence of rod focal length. This is shown more clearly by differentiating equation 2.1 for W_2 with respect to g_2;

$$\frac{dW_2}{W_2} = \frac{1}{4} \cdot \frac{(2g_1g_2-1)}{(1-g_1g_2)} \cdot \frac{dg_2}{g_2} \qquad 2.3$$

Clearly, as $g_1g_2 \rightarrow 1$, W_2 becomes sensitively dependent on g_2. If W_2 (the spotsize within the rod) is varying, then varying amounts of energy will appear in the TEM_{oo} mode output of the laser, thus rendering it a rather unsatisfactory device. It was Steffen, Lörtscher and Herziger (1972) who first pointed out this important effect, but they also pointed out the fact that if $g_1g_2 = \frac{1}{2}$ then in the numerator of equation 2.3 we have $(2g_1g_2-1) = 0$ and the spotsize W_2 is now relatively insensitive to fluctuations in g_2 even when it is made very large. They referred to resonators that could be designed with this property incorporated at "dynamic stable resonators" and gave a number of examples which they had tried and tested. These will not be gone into here except to mention that they suggested incorporating a telescope within a cavity. They appear not to have tried this experimentally and it was left to Sarkies (1979) to report the first use of such a design. Although he did not obtain TEM_{oo} mode operation due to a none optimum choice of telescopic magnification, he did obtain a good working compromise between the requirements of low beam divergence and high power, damage free operation.

It is shown in the next section that a correct choice of telescope does satisfy the $g_1 g_2 = \frac{1}{2}$ criterion of Steffen et al and should therefore result in a stable, high energy, TEM_{oo} mode output.

2.2 Theory of Telescopic Resonator

The theory of the telescopic resonator has been presented in great detail elsewhere (Hanna, Sawyers, Yuratich (1981); Sawyers (1981); Berry (1982)) and so a very brief summary will be given here. It will be split into two parts. The first part will cover the analysis of the TEM_{oo} spotsizes formed within the telescopic resonator cavity and the second part will be concerned with a theoretical analysis of how the TEM_{oo} mode is selected in preference to any other higher order transverse mode.

2.2.1 Analysis of the TEM_{oo} Mode Spotsizes

The general telescopic resonator is shown in fig. 2.1. The mirrors at either end are assumed curved and are then treated as lenses of focal length R in front of plane mirrors. This allows treatment of the resonator analysis in the normal way in terms of single-pass ray matrix elements. From fig. 2.1 it is clear that there are nine elements to be considered i.e. five lenses and four spaces. The cavity could be analysed by multiplying together the nine ray matrices to obtain the full single pass ray matrix and then applying the theory outlined in Baues (1969) to obtain the spotsizes at either end. Indeed, we have developed a computer programme that can do just this and which can give the spotsize and radius of curvature at any element within the cavity.

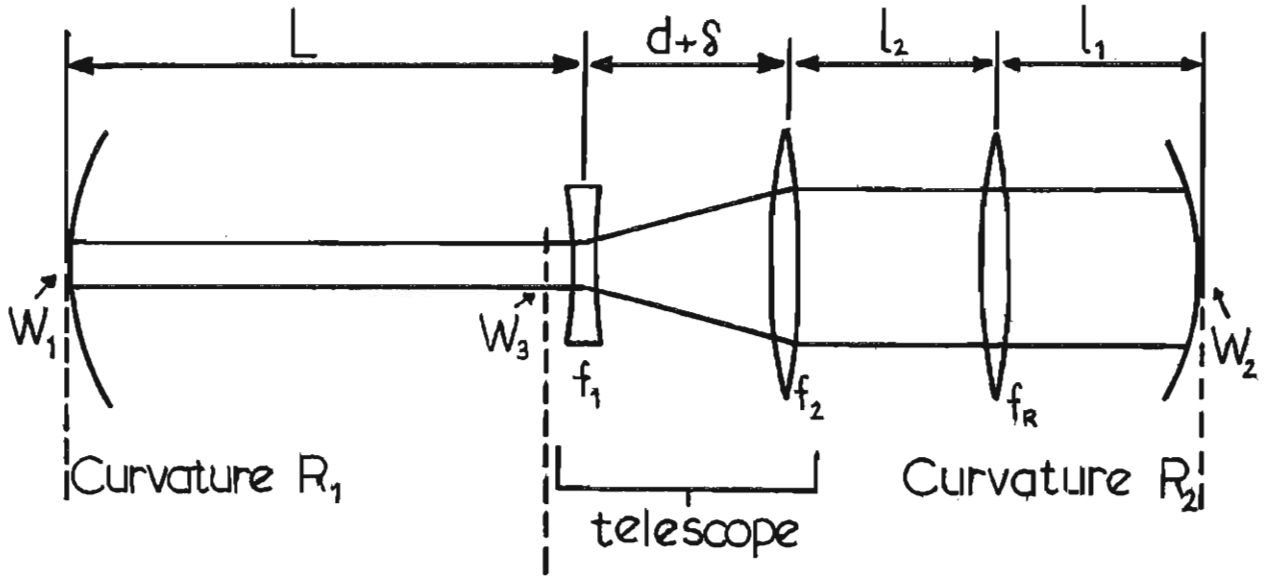

Figure 2.1: The general telescopic resonator.

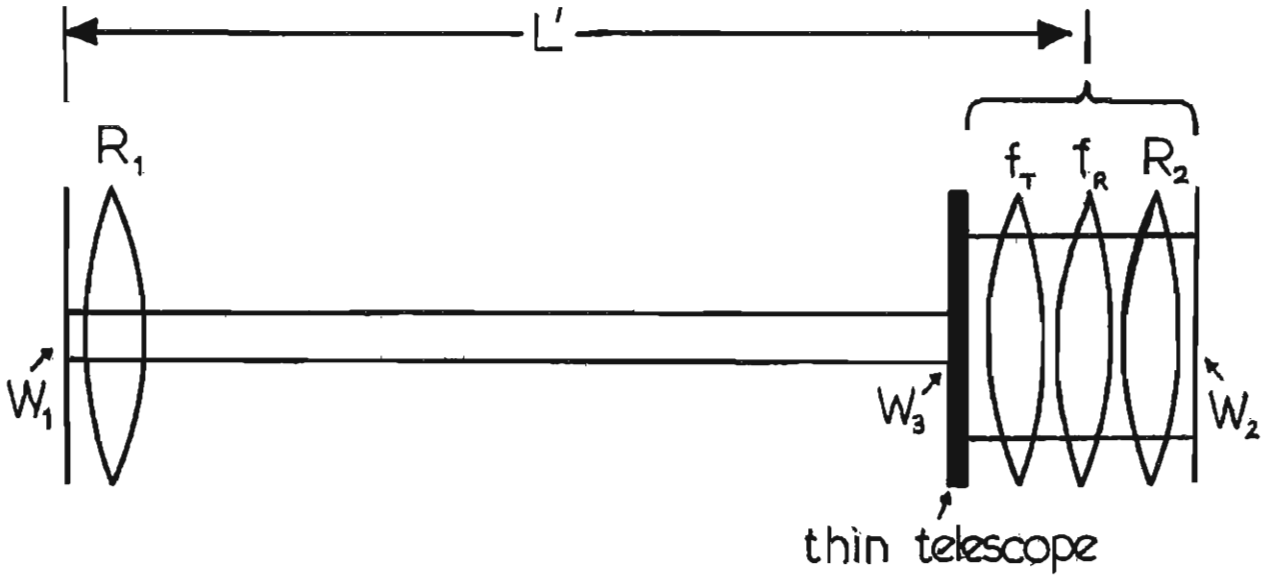

Figure 2.2: Equivalent resonator for the simplified telescopic resonator.

This approach is obviously less useful than one which provides simple equations which can be used to design the resonator. It does, however, provide a good test of the accuracy of the predictions of any simplified analysis. We now consider how such a simplified analysis can be developed.

To begin with certain simplifications are made which can be relaxed later. These are that the rod is adjacent to mirror 2 (i.e. $l_1 = 0$) and that it is also in the focal plane of the telescope objective ($l_2 = f_2$). Simple but exact expressions can then be derived for the spotsizes.

Hanna et al (1981) show that the ray matrix for the telescope comprising the lens f_1, the space $d + \delta$(where $d = f_1 + f_2$) and the lens f_2 can be written as a combination of four matrices;

$$\begin{bmatrix} 1 & -f_2 \\ 0 & 1 \end{bmatrix} \begin{bmatrix} 1 & 0 \\ -1/f_T & 1 \end{bmatrix} \begin{bmatrix} M & 0 \\ 0 & 1/M \end{bmatrix} \begin{bmatrix} 1 & -f_1 \\ 0 & 1 \end{bmatrix}$$

Thus, instead of matrices for a lens, a space and a lens it now looks like a space of length $-f_1$, a "thin telescope", a lens of focal length f_T, where we shall see that $f_T = f_2^2/\delta$, and another space of length $-f_2$. Combining this with the other elements from fig. 2.1 we have the equivalent resonator shown in fig. 2.2.

The sequence of elements is now; a lens of focal length R_1; a space $L' = L - f_1$; a thin telescope; a lens pair f_T and f_R separated by a space $l_2 - f_2 = 0$ in our special case; and finally a lens of focal length R_2. The last three elements can be combined into a single lens element of focal length R_2' where;

$$\frac{1}{R'_2} = \frac{1}{f_T} + \frac{1}{f_R} + \frac{1}{R_2} \qquad 2.4$$

So we are left with only four ray matrices for the single-pass resonator and these can easily be multiplied together to give the single-pass matrix;

$$\begin{bmatrix} A & B \\ C & D \end{bmatrix} = \begin{bmatrix} G_1 & ML' \\ \dfrac{-(1-G_1G_2)}{ML'} & G_2 \end{bmatrix} \qquad 2.5$$

where the new G-parameters are:

$$G_1 = M \cdot \begin{bmatrix} 1 & - & \dfrac{L'}{R_1} \end{bmatrix} \qquad 2.6$$

$$G_2 = \frac{1}{M} \cdot \begin{bmatrix} 1 & - & \dfrac{M^2L'}{R'} \end{bmatrix} \qquad 2.7$$

We can now express the spotsizes W_1, W_2 in the normal way as shown by Baues (1969). If these are expressed as W_1' and W_2', normalised with respect to L', we obtain;

$$W_1' = \left[\frac{\pi W_1^2}{\lambda L'}\right]^{\frac{1}{2}} = \left[\frac{M^2 G_2}{G_1(1-G_1G_2)}\right]^{1/4} \qquad 2.8$$

$$W_2' = \left[\frac{\pi W_2^2}{\lambda L'}\right]^{\frac{1}{2}} = \left[\frac{M^2 G_1}{G_2(1-G_1G_2)}\right]^{1/4} \qquad 2.9$$

$$W_B' = \left[\frac{\pi W_3^2}{\lambda L'}\right]^{\frac{1}{2}} = \left[\frac{W_2'}{M}\right] \qquad 2.10$$

These are plotted in fig. 2.3 when G_1 and M are kept fixed, G_2 being varied. Varying G_2 can represent changes in telescopic defocussing δ via R_2' or changes in rod focal length f_R, also via R_2'. The most important point to note is that the variation in W_2' is least when $G_2 = \frac{1}{2}G_1$, showing that the telescopic resonator, when correctly designed, is indeed, a "dynamic stable resonator". Since there is no advantage to be gained from having curved mirrors (indeed making R_1 plane allows us to use an uncoated resonant reflector and so increase the power handling capability of the narrow beam end of the resonator) the equations can be simplified by putting $R_1 = R_2 = \infty$. They become (also using equations 2.6 and 2.7), with $G_1\ G_2 = \frac{1}{2}$, $G_1 = M$, $G_2 = 1/2M$

$$W_1 = \left[\frac{\lambda L'}{\pi}\right]^{\frac{1}{2}} \qquad 2.11$$

$$W_2 = \left[\frac{\lambda L'}{\pi} \; .2M^2\right]^{\frac{1}{2}} \qquad 2.12$$

$$W_3 = \left[\frac{2\lambda L'}{\pi}\right]^{\frac{1}{2}} \qquad 2.13$$

These equations are the basic design equations for the telescopic resonators used in the work for this thesis. As can be seen the small beam spotsize W_1 really only depends on the spacing between end plane mirror and telescope. After this has been fixed the spotsize W_2 in the rod can be made any size by choosing a suitable magnification M. Thus, the TEM_{oo} mode can be made to fill the rod completely, whilst at the same time being insensitive to fluctuations in G_2. It is apparent, therefore, that the telescopic resonator should be able to produce stable, high energy TEM_{oo} mode outputs.

It must not be forgotten, however, that certain approximations were made at the beginning of this analysis. It is shown in Hanna, Sawyers, Yuratich (1981), however, that relaxing these two approximations (that $l_2 = f_2$ and $l_1 = 0$) only results in very small changes in the definition of R_2' as given by equation 2.4.

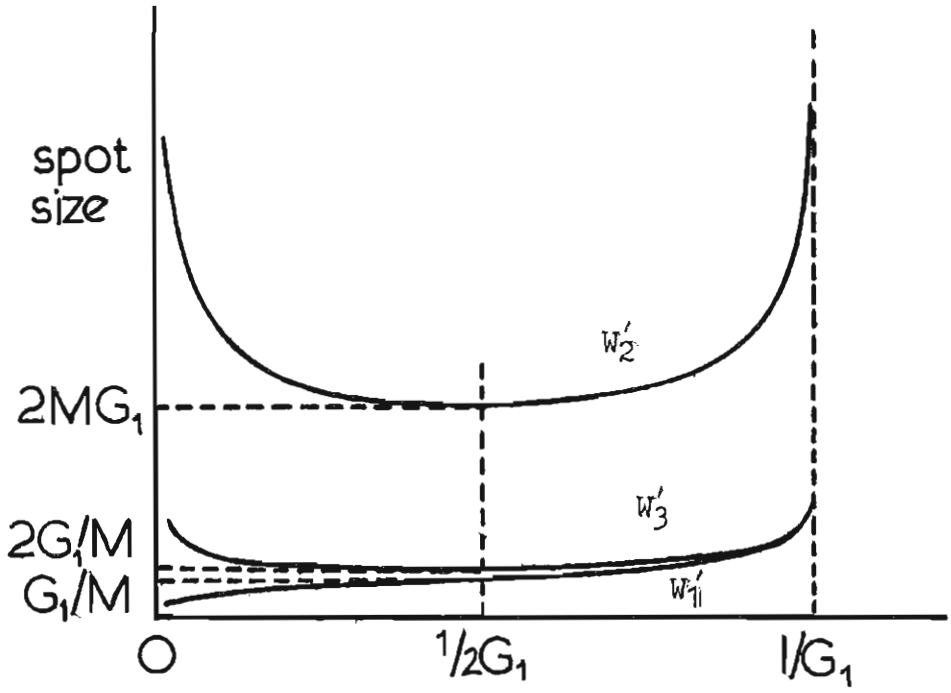

Figure 2.3: Normalised spotsizes W_1', W_2' and W_3' versus G_2 for fixed G_1 and magnification M.

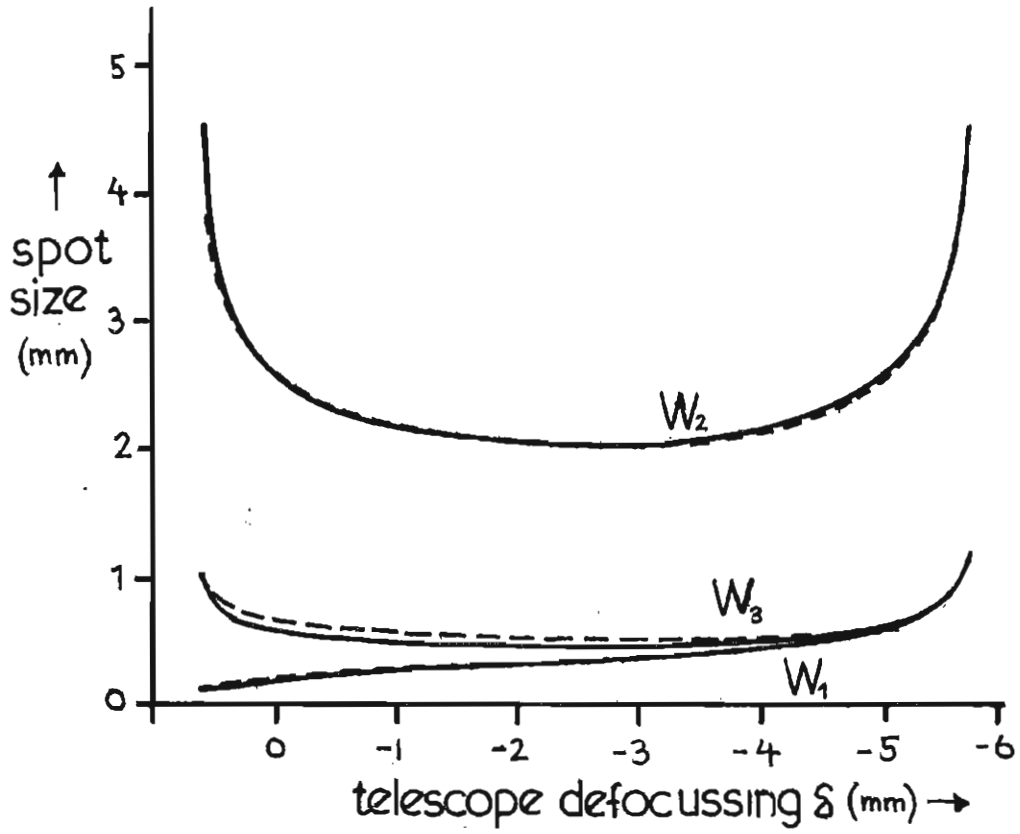

Figure 2.4: Calculated spotsizes versus telescope defocussing using typical operating parameters for a 9.53mm rod as indicated in table 2.2. Solid curve was obtained using exact ray transfer matrices and the dashed curve using the theory of section 2.2.1.

In all practical cases, therefore, (especially when R_2 is plane) these changes can be ignored and the equations already presented can be used with confidence. As proof of this, a comparison was made between the spotsize predictions of the theory presented above and a computer performed multi - plication of all the individual elements in a typical telescopic resonator. The two sets of curves are shown in fig.2.4. As can be seen the agreement is excellent.

2.2.2 Theory of Transverse Mode Selection

We have so far developed a theory that predicts the TEM_{oo} spotsizes within the cavity. We now need to apply sufficient transverse mode selection to ensure that this mode is the only one allowed to oscillate or at least is the dominant mode. This is achieved using a circular aperture at one end mirror (usually, for convenience, at the large beam end) which, over typical numbers of round trips (say, at least, a few tens of round trips even for fast Q-switched operation) provides sufficient discrimination against the TEM_{o1} and other higher order modes by introducing a large loss for these modes whilst only introducing a small loss for the TEM_{oo} mode. The round trip losses for such an aperture, L_{oo} and L_{o1} for TEM_{oo} and TEM_{o1} respectively, can be found exactly using the results of Li (1965). From this work it is also worth noting that confocal resonators offer the best discrimination between TEM_{oo} and TEM_{o1}. It is shown by Sawyers (1981) that any "dynamic stable resonator", such as the telescopic resonator, is equivalent to an empty confocal resonator provided the aperture is at one end mirror.

Thus, the telescopic resonator has the maximum discrimination between the desired TEM_{oo} and any other mode. So the aperture selection procedure is to pick one that barely truncates the TEM_{oo} mode, and then check from the work of Li that over typical numbers of round trips this size provides adequate discrimination. In practice, the relation $2a = 3W$ is satisfactory, where a is the radius of the aperture. This condition is used in all our resonators. We have now presented all the theory necessary to build a stable, high energy, TEM_{oo} mode laser. It will be shown in the next section how such a resonator can produce a high power in a single longitudinal mode when Q-switched in an appropriate way.

2.3 Theory of High Power and Narrow Linewidth Operation

It is well known that high powers in a single pulse can be obtained by Q-switching, where lasing is prevented by some intra-cavity loss until a large population inversion and therefore gain has built up at the end of the flashlamp pulse, at which point the intra-cavity loss is suddenly reduced thereby allowing the rapid build-up of a giant, high-power pulse in a time corresponding to a few tens of cavity round trips. We refer to this conventional form of Q-switching as "fast" Q-switching. For the telescopic resonator this number of round trips is sufficient to ensure selection of the desired transverse mode, i.e. the TEM_{oo} mode, as described in the previous sections.

So one is now in a position to build a stable, high energy, high power TEM_{oo} output laser. It only remains to frequency narrow this output down to a single longitudinal mode (SLM). The problem here is that frequency narrowing can only be conveniently obtained from frequency selection elements that only provide a small amount of discrimination between adjacent longtiduinal modes per cavity round trip. In fast Q-switched operation there are only a few tens of round trips available for this selection to occur, insufficient to reliably narrow the output down to a single longitudinal mode on more than just the odd shot. Clearly, what is needed is a very long intra-cavity pulse build-up time, equivalent to hundreds of round trips. This can be provided by the technique of pre-lase Q-switching. (Hanna et al, 1972 a, b).

2.3.1 Theory of Pre-Lase Q-Switching

In pre-lase Q-switching the cavity losses are arranged by adjustments of the Pockels cell voltage to be only just less than the peak gain reached during the flashlamp pulse. A small net gain is therefore reached at the peak of the inversion and this results in a very long build-up time for the intra-cavity radiation, analogous to the situation where a saturable absorber Q-switch is used. During this build-up time there can be many hundreds of passes through a frequency selective element, enough to narrow down the linewidth to a single longitudinal mode.

If the losses are set at the correct level the build-up starts towards the end of the flashlamp pulse and the laser radiation then builds up to a detectable level very near to the end of it. If the losses are then suddenly reduced we are left with a very large gain which results in the rapid build up of a giant high power pulse in the same way as fast Q-switching. The difference is that now, instead of starting from noise, the build-up is from the single longitudinal mode already established within the cavity. As a result the high power output is also SLM. To actually calculate the amount of mode selection necessary we must consider the powers developed in the various longitudinal modes. It can be shown (Sawyers 1981) that if a mode n reaches threshold at time t_n and then continues to grow over q_n round trips each of time τ the power P_n in that mode is given by;

$$P_n(t_n + q_n\tau) = P_{no}(R_{1n}R_2)^{q_n} \exp\left[2\sigma_n l \sum_{p=1}^{q_n} N(t_n + (q_n-p)\tau)\right] \quad 2.14$$

where P_{no} is the noise power in mode n, σ_n is the stimulated emission cross-section for the n'th mode, l is the length of the lasing medium and N(t) is the population inversion at a time t. R_{1n} and R_2 are the resonator mirror reflectivities where R_2 is assumed the same for all modes and the effect of the mode selective elements has been modelled by a mirror reflectivity R_{1n} which is dependent on the mode number n.

For fast Q-switching the inversion can be assumed constant over the few tens of round trips of build-up and so equation 2.14 reduces to;

$$P_n(t) = P_{no} (R_{1n}R_2)^{q_n} \exp \left\{ 2\sigma_n l N(t_s) q_n \right\} \qquad 2.15$$

where t_s is the time at which switching occurs. Comparing equation 2.15 with a similar expression for mode m it becomes clear that the terms in the exponential describes the normal gain narrowing whereas the term $(R_{1n}R_2)^{q_n}$ accounts for an extra narrowing due to the frequency selection elements. The importance of this second term is increased dramatically in pre-lase Q-switching where q_n is made much larger than it is in fast Q-switching. In pre-lase Q-switching we aim to select a single longitudinal mode and so we are primarily concerned with the ratio of powers for two adjacent cavity modes. For two such modes the stimulated cross-sections are approximately equal and so gain narrowing is relatively unimportant compared to the narrowing introduced by the frequency selective elements. A further complication is that we can no longer approximate the inversion to a constant since we are dealing with long build-up times. We do, however, assume that it can be approximated by a linear relationship over the duration of the build-up;

$$N(t) = \gamma t - \mu \qquad 2.16$$

where $\gamma = dN(t)/dt$ is the pumping rate.

Using equation 2.16 in equation 2.14 it can be shown, after some manipulation, that the power in two adjacent modes n and m is given by;

$$\frac{P_n(t_s)}{P_m(t_s)} = \left[\frac{R_{1_n}}{R_{1_m}}\right]^{q_{eff}} \qquad 2.17$$

Where;

$$q_{eff} = \frac{q_n + q_m}{2} = q_n - \frac{\epsilon}{4\sigma(\omega_o)\gamma_1 T} = \left[\frac{\ln(Pn/Pno)}{\sigma(\omega_o)\gamma_1 T}\right]^{\frac{1}{2}} - \frac{\epsilon}{4\sigma(\omega_o)\gamma_1 T} \qquad 2.18$$

Here we have assumed that mode n reaches threshold first, that $\sigma_n \approx \sigma_m = \sigma(\omega_o)$ and that R_{1_n}/R_{1_m} can be written in the form $1 + \epsilon$. These last two equations are the basic results of the theory of pre-lase Q-switching. For SLM operation we require a certain ratio of power between the main mode n and an adjacent mode m. This sets the LHS of equation 2.17. The ratio R_{1_n}/R_{1_m} is determined by the mode selector chosen, as is q_{eff} via the factor ϵ in equation 2.18. More importantly, however, the value of q_{eff} depends on the lasing medium itself, and particularly on the rate of change of population inversion γ.

2.3.2 The Application of Mode Selection

It is well known that etalons and resonant reflectors have frequency dependent transmissions and reflectivities respectively.

It is shown in Sawyers (1981) that the frequency selectivity of either device can be cast into the form of the frequency dependent reflectivities $R_{1n,m}$ used in the previous sections. The results are merely quoted here;

$$\frac{R_{\omega_o}}{R_{\omega}} = 1 + \epsilon \qquad 2.19$$

Where, for an etalon used in transmission;

$$\epsilon = \epsilon_T = \left(\frac{\pi\Delta}{\Delta_E}\right)^2 \quad (C_E - 1) \qquad 2.20$$

and for a resonant reflector;

$$\epsilon = \epsilon_R \simeq \left(\frac{\pi\Delta}{\Delta_E}\right)^2 \left(\frac{1}{C_E}\right) \qquad 2.21$$

Here mode n has frequency ω_o and is placed at the transmission or reflection peak respectively. Mode m is at a frequency ω where $\Delta = \omega_o \pm \omega$. Δ_E is the free spectral range of the etalon or resonant reflector and C_E is the contrast. If we could ensure that mode n was always at the centre of the transmission or reflective peaks then equations 2.20 and 2.21 would complete the theory.

Unfortunately, the resonator mode frequencies are generally moving around randomly relative to these peaks, resulting in randomly varying degrees of mode selection necessarily less than the amount predicted by equations 2.20 and 2.21. The general situation is depicted in fig. 2.5. At this point it is necessary to agree on a definition for single-mode operation. The most convenient is to define it as a certain power ratio between the two highest power adjacent cavity modes (i.e. the two nearest the reflectivity maximum as depicted in fig. 2.5).

$$\text{Thus} \quad \frac{P_n}{P_m} = \frac{P_n}{P_{n\pm1}} = N \qquad 2.22$$

Where N is arbitrarily set at some agreed value. In our work SLM operation is determined by checking to see that there is less than 1% beat modulation on the temperal profile of a pre-lase Q-switched output pulse. It can be shown (Hanna et al, 1981) that for a ratio K of beating amplitude to mean power without beating the ratio of powers in the two modes is given by

$$N \approx \frac{16}{K^2} \qquad 2.23$$

Thus, even for 1% beating ($K = 0.01$) we have $N \approx 10^5$. Referring to fig. 2.5, it is apparent that there is an upper limit on ΔL_n beyond which equation 2.23 will not be satisfied after the available number of cavity round trips.

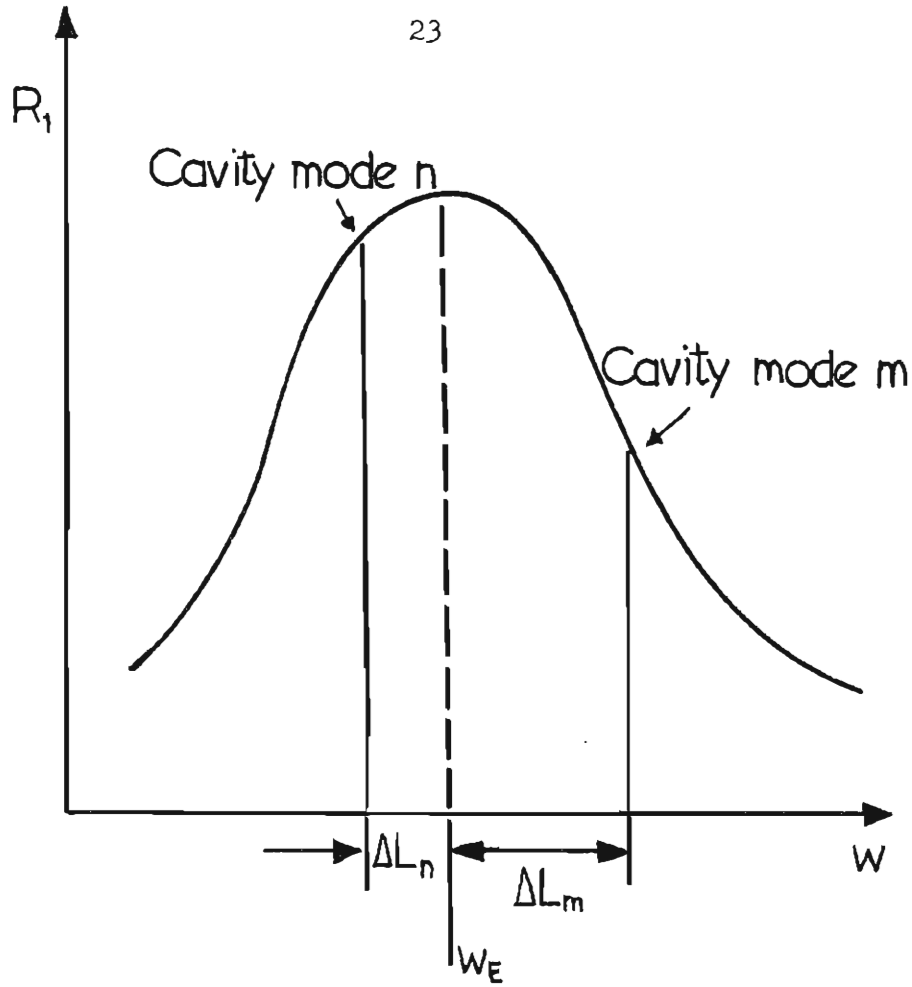

Figure 2.5: General location of two cavity modes m and n relative to a reflectivity maximum of a mode selector.

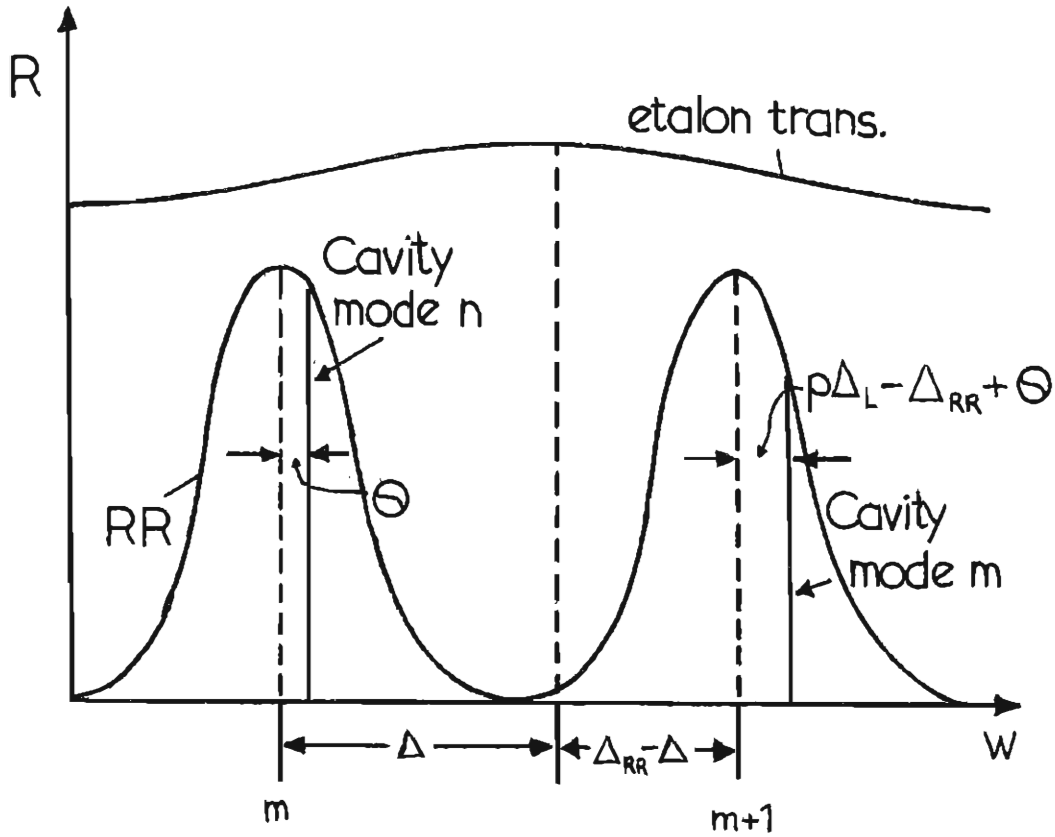

Figure 2.6: General location of two cavity modes n and n+p relative to two reflection maxima of a resonant reflector and a transmission maximum of an intra-cavity etalon.

Thus, if mode n is fluctuating randomly but symmetrically about the reflectivity maximum we can work out an expression for the ratio of single-mode shots defined by equation 2.23 to shots that contain an unacceptable degree of mode beating. The ratio is (Hanna and Koo,1982)

$$r = \epsilon \left(\frac{q_{eff}}{\ln N} \right) - 1 \qquad 2.24$$

It is clear that unless we can completely stabilise the cavity modes then this equation represents a fundamental limitation on the number of shots that can be SLM. Even if the mode selectivity is very high there will always be some occasions when two adjacent modes fall symmetrically about the reflectivity maximum.

Further complications arise when the more practical problems of applying mode selection are considered. Theoretically the intra-cavity etalon provides the best approach to obtaining a large selectivity since ϵ_T can be made arbitrarily large by increasing R. In practice, however, such an etalon must be tilted by a significant amount to prevent lasing from its surfaces. This tilt degrades the finesse and increases the insertion losses. One solution to this problem is to place a $\lambda/4$-plate either side of the etalon and place this whole assembly the other side of a polariser from the laser rod.

The etalon can then be used at, or very near to, normal incidence. This technique is described in Hanna, Koo, Pratt (1983). A simpler approach is to use a thick resonant reflector to do the adjacent mode selection. The advantage here is that a resonant reflector is used as the end mirror in the narrow beam end of the telescopic resonator anyway because, being uncoated it has the necessary high damage threshold. The problem with this approach is that to get sufficient selection between two adjacent modes the resonant reflector (RR) must be very thick (75mm in our case) and this thickness results in a very small free spectral range. It is then possible to have lasing on two cavity modes each of which are now near the reflection maxima of two adjacent RR reflection maxima. Such two-mode operation could go un-noticed if the sole diagnostic of SLM was the observation of modulation on the pulse displayed on an oscilloscope since this high frequency beat would not be detectable. The situation is depicted in fig. 2.6. Also shown on the diagram is the transmission maximum of a low finesse etalon. Such an etalon can be introduced to provide enough mode selection to discriminate between the two RR reflection maxima. Thus, if we have two cavity modes n and n+p (where p is an integer), n is at a frequency offset θ from RR maximum m and n+p is at a frequency offset $p\Delta L - \Delta_{RR} - \theta$ from RR maximum n+p where ΔL is the cavity mode spacing and Δ_{RR} is the FSR of the RR, then it can be shown (Berry, 1982) that the overall discrimination between the two cavity modes is;

$$\frac{R(m,n)}{R(m+1,\ n+p)} = \left\{\frac{1+F\sin^2\left[2\pi nt(\Delta_{RR}+\Delta)\right]}{1+F\sin^2\left[2\pi nt\Delta\right]}\right\}^2 \left\{\frac{1+\left(\frac{p\Delta L - \Delta_{RR} + \theta}{\Delta_{RR}}\right)\frac{\pi^2}{C_E}}{1+(\theta/\Delta_{RR})\cdot\frac{\pi^2}{C_E}}\right\} \qquad 2.25$$

where the first term in brackets refers to the RR, the second to the etalon and all the symbols have their normal meanings. This equation, in conjunction with equation 2.17, indicates whether there is adequate discrimination between cavity modes in adjacent RR reflection maxima as well as between adjacent modes in one RR reflection maximum. This also completes the theory of mode selection necessary for its application to the telescopic resonator.

2.4 Design and Operation of Fixed-Q and Fast Q-Switched Telescopic Resonators

As mentioned at the beginning of the chapter the theory of the previous sections has been used to design telescopic resonators around three different commercially available Nd:YAG rod sizes. The rods were all cylindrical with parallel end faces and had the following dimensions; 9.53mm by 75mm, 6.35mm by 75mm and 4.00mm by 75mm. The largest rod was pumped by twin flashlamps each cpable of 50 Joule output at up to 20Hz. The two smaller rods were pumped by only a single flashlamp (capable of up to 50 Joule output) and therefore only half the energy input per pulse of the big rod.

Basically there are only two design requirements. The first is to ensure that that the TEM_{oo} mode fills as much of the rod aperture as possible without coming dangerously close to its edges. We therefore choose an aperture of diameter d a millimetre or so less than the rod diameter. The aperture diameters used were 7mm, 5.2mm and 3.5mm for the three rod sizes respectively. Having chosen these sizes the equation $d = 3W$, as discussed in section 2.2.2 on transverse mode selection, gives us the required TEM_{oo} spotsizes W_2.

The second design requirement is to choose a contracted beam spotsize W_1 that allows us to extract a high power output from the resonator. Experience during development has shown that if the end mirror is an uncoated resonant reflector then a spotsize of around 0.4mm can safely pass 100mJ in 25ns (i.e. when fast Q-switching) at the same time as allowing a convenient overall cavity length of around 1m.

These two requirements are related and fix the design of the resonator via the two equations 2.11 and 2.12 which are repeated here;

$$W_1 = \left(\frac{\lambda L'}{\pi}\right)^{\frac{1}{2}} \qquad 2.11$$

$$W_2 = \left(\frac{\lambda L'}{\pi}\right)^{\frac{1}{2}} . M\sqrt{2} \qquad 2.12$$

Fixing W_1 determines the length $L' = L + f_1$, and this length, when substituted into equation 2.12, determines magnification M necessary to give the required value for W_2. Performing this operation for the three rods in question we obtain the following tables of results:

Table 2.1 Design parameters for the three rod sizes used

Rod diameter (mm)	Aperture (mm)	W_2 (mm)	W_1 (mm)	L' (cm)	M
9.53	7.00	2.33	0.41	50.0	4
6.35	5.20	1.73	0.41	50.0	3
4.00	3.50	1.17	0.41	50.0	2

Obviously, the exact aperture sizes have also been chosen to allow conveniently achievable magnifications to be used.

The general arrangement of all three resonators is the same as that of fig.2.1. The actual parameters relevant to that diagram for the three rods are presented in the table below:

Table 2.2 Experimental parameters for the three rod sizes used

Rod diameter (mm)	L (cm)	f_1 (cm)	f_2 (cm)	L_2 (cm)	f_R (m)	L_1 (cm)
9.53	46.66	-3.33	+13.33	35	6	20
6.35	45.00	-5.00	+15.00	30	5	25
4.00	40.00	-10.00	+20.00	30	4	25

Note that all three cavities can easily be made the same overall length of about 105 cm. It was the parameters presented above for the 9.53mm rod that were used to obtain the full matrix element, computer calaculated spotsize results which were used as a test of the theory of section 2.2.1, the parameters for the latter being taken from table 2.1.

Figure 2.4 showed the excellent agreement between the two approaches and so it now only remains to demonstrate that the theoretically calculated spotsizes are obtained in practice.

All three rods were run fixed-Q in basically the same configuration as shown in fig.2.1, but with a polariser and aperture in the large beam end of the cavity. The telescope itself was first set in normal adjustment during the initial alignment, and then optimised whilst the laser was running to produce maximum energy output. When running fixed-Q the output could be taken from either end of the cavity, the other end having the 100% plane mirror. In all cases the far-field spatial profiles were found to be TEM_{oo} with spotsizes that corresponded to those expected from the theoretically predicted waist-sizes at the output mirrors of the laser. This behaviour was revealed by diode array measurements and also by very clean circular burn patterns on photographic paper. Typical results are shown in figs. 2.7 and 2.8, in this case for the 9.53mm rod taking the output from the narrow beam end. All the rods could give 100mJ outputs, the smallest giving ~200mJ at the full 50Joule input and still remaining TEM_{oo}. It is clear, therefore, that fixed-Q operation performs in accordance with theory. The next step is to operate the resonators fast Q-switched. This involves the addition of a Pockels cell to the cavity which is used in conjunction with the polariser already present. The high powers involved in fast Q-switching require that mirror 1 at the narrow beam end be uncoated to avoid damage. As a result this end is invariably the output end with an uncoated resonant reflector serving as the cavity mirror.

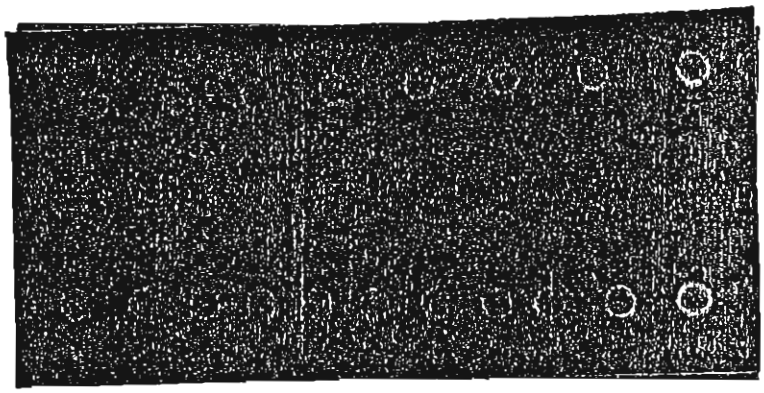

Figure 2.7 : Typical far-field burn patterns for ~100mJ fixed-Q pulses taken from the contracted beam end of a cavity employing a 9.53mm diameter rod.

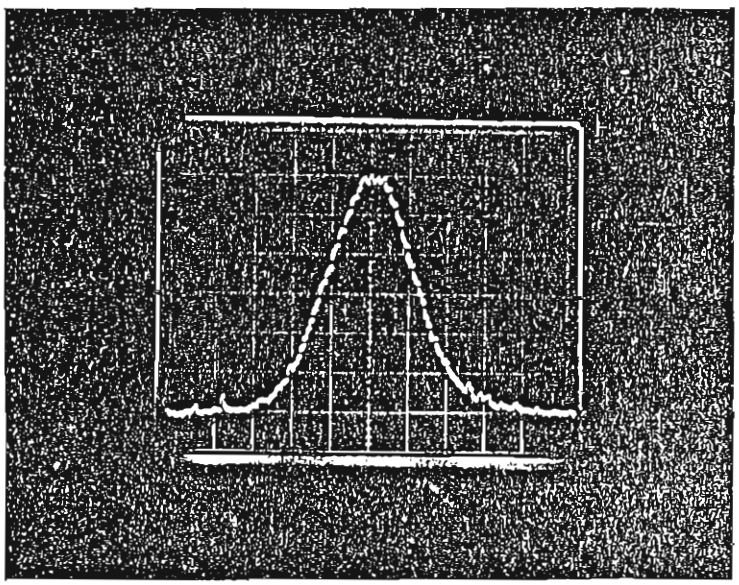

Figure 2.8 : Diode array picture of the spatial profile of the fixed-Q pulses shown in figure 2.7.

All the rods could provide 100mJ, 20-25ns (FWHM) pulses in this configurtion (only just for the 4mm rod, ASE being a problem for harder pumping) with the Pockels cell and polariser placed either side of the rod. A point worth mentioning here is that if Pockels cell hold-off is a problem as a result of thermally induced birefringence in the rod then it is better to place the Pockels cell and polariser between the rod and the 100% mirror, rather than at the other side of the rod. This is more likely to be the case with the smaller, higher gain rods. The output beams were all found to be TEM_{oo}, the photographic burn patterns and diode array traces looking just the same as those of figs. 2.7 and 2.8. The power output was only limited by damage to the narrow beam end mirror. As mentioned above, an uncoated resonant reflector was used to maximise this value, but for our 0.41mm spotsize damage still occurs at power levels of about 150mJ in 20ns (FWHM) fast Q-switched pulses. Everyday operation is therefore kept to around 100mJ output. Some attempt has also been made to operate the telescopic resonator Q-switched whilst taking the output from the large beam end. This implies some form of 100% mirror at the narrow beam end of the cavity. A normal multi-layer coated 100% mirror, however, could be damaged by the high powers. Carr and Hanna (1982) have used an anti-resonant ring prism arrangement as the 100% mirror in the hope that its damage threshold would be high due to the fact that it uses no coated surfaces. Although it worked well as a 100% mirror its damage threshold was only about twice that of a coated mirror due to standing wave effects and therefore only allowed a damage free output of around 150mJ from the large beam end. The output was, however, the usual diffraction limited TEM_{oo} mode in the far-field.

It is clear, therefore, that the telescopic resonator theory of the previous sections provides an excellent design procedure for the building and operation of a stable energy, high power diffraction limited TEM_{oo} mode laser which is of a convenient length and easy to use. We now describe the performance of this laser when operated in a single longitudinal mode.

2.5 Operation of the Telescopic Resonator using Pre-Lase Triggered Q-Switching

The pre-lase Q-switched operation of the telescope resonator was first reported in Berry, Hanna, Sawyers (1981) and a copy of this paper is reproduced in appendix 1. As can be seen in this paper, the pre-lase is monitored by a PIN photodiode. This detects cavity radiation rejected by the polariser either as a result of depolarisation in the rod (Appendix 1, Fig.1), or better, as a result of the Pockels cell induced depolarisation which would come off the polariser in the opposite direction than that shown in the diagram. The latter is a much better approach since, when the Pockels cell is fully opened, there is no depolarisation in this direction and the PIN photodiode is protected from the full power of the Q-switched pulse.

2.5.1 Calculation of the Degree of Mode Selection

If we require less than 1% beating on a smooth Gaussian temporal profile then equation 2.23 tells us that we need at least a power ratio of 1.6×10^5 between our main mode and any other mode, particularly the adjacent modes.

We therefore expect a ratio of SLM to multimode shots of; (from equation 2.24)

$$r = \epsilon \left(\frac{q_{eff}}{\ln(1.6 \times 10^5)} \right) - 1$$

ϵ is given by equations 2.20 and 2.21 for an etalon and resonant reflector respectively. q_{eff} is given by equation 2.18 and depends on known quantities, except for the parameter γ, the rate of change of population inversion. Ways must be found, therefore, of obtaining values for this quantity before the necessary degree of mode selection can be calculated. It must be remembered here that the theory assumed a linear rate of change of population inversion, an assumption that is clearly only an approximation since we are operating near the maximum of a peaked inversion-against-time curve. In Berry (1982) three methods are proposed for the evaluation of γ, each one having various problems and therefore possible errors associated with it, these also being outlined. Nevertheless, it is a fact that the third of these methods, which involves observing the time at which a Q-switched pulse appears as a function of flashlamp energy, does give a reasonably accurate value for γ , and indeed one which leads to good agreement between predictions from the theory and experimental results. In short, therefore, the theory outlined above provides an adequate prescription for choosing the necessary mode selection to observe SLM behaviour.

2.5.2 Pre-Lase Triggered, Q-switched Operation

It is convenient to look at the three rod sizes separately and consider the types of mode selection applied to each one.

a) The 9.53 mm Rod

The large rod had mode selection applied to it in the two ways depicted in fig. 2.9, in both of which the output is taken from the narrow beam end. In design (11) the intra-cavity etalon is typically 1 cm thick and has 65% face reflectivities. Equation 2.20 predicts $\epsilon_T = 0.075$. Our best estimate of γ from the previous section is then used in equation 2.18 to predict $q_{eff} = 465$. These values then predict 66% of shots being SLM using equation 2.24. The 1/4" thick resonant reflector included in this configuration has two features which contribute to the resonator design. First, it provides a high damage threshold reflector of high output coupling (14% relectivity). It also provides the necessary discrimination between transmission maxima of the intra-cavity etalon.

In design (1) the adjacent mode discrimination is provided by a thick resonant-reflector output mirror. Equation 2.21 predicts $\epsilon_R = 0.0833$ which by the same procedure as before also predicts $\sim$66% of shots being SLM. Here, however, we need the additional, low finesse intra-cavity etalon to discriminate between adjacent resonant reflector maxima, and these two selective elements must be temperature stabilised to about $0.1^{\circ}C$. Calculations using equation 2.25 reveal that a 1/4" thick, 20%/20% face reflectivity etalon is adequate.

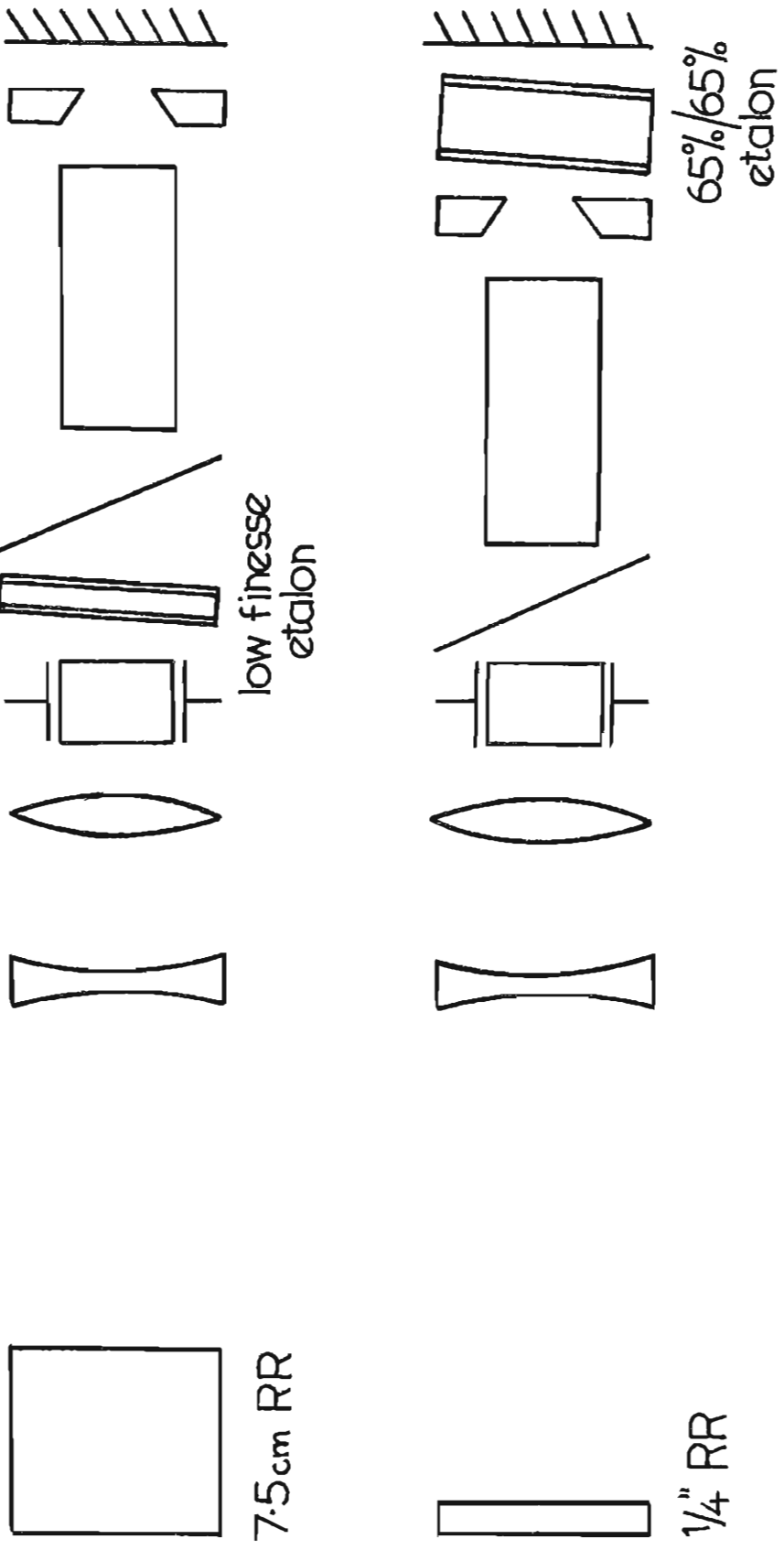

Figure 2.2: The two methods of mode selection used for the 9·53mm diameter rod.

The two cavities were both operated successfully at the 100mJ, 30ns (FWHM) level. When the Pockels cell opening was deliberately lengthened to a time of order 75ns the SLM temporal pulse profiles were complely smooth as shown in appendix I, fig. 3(a). For the two cavities the ratio of SLM to multimode shots was indeed around 66% or somewhat better. A typical performance was 1.5 minutes of SLM pulses at 12Hz, followed by some 30 seconds of beating. This performance allowed the traces of 250 consecutive shots to be recorded on a storage scope. As shown in the appendix I, fig. 3(b) the output energy is seen to be very stable under these SLM conditions.

b) The 6.53mm Rod

To date the 6.53 mm rod has only been operated using design (11) of fig. 2.9, the same type of etalon and resonant reflector being used as for the 9.35mm rod. 100mJ output is possible using very near to the full 50Joule input from the single flashlamp, although normal everyday operation tends to be around 80mJ (Ian Carr, private communication). Although no calculation of γ has been made for this rod it is expected to be greater than for the 9.35mm rod since the inversion density must be greater. This would result in a lower value for q_{eff} which in turn leads one to expect a somewhat smaller ratio of SLM to multimode shots. This is indeed seen to be the case.

c) The 4.00mm Rod

Work on the 4.00mm diameter rod was performed during a short visit to J K Lasers Ltd and is therefore less extensive than work on the other two rod sizes. The mode selection was again only applied as in design (11) of fig. 2.9. With the Pockels cell and polariser between the rod and telescope it was found to be impossible to prevent Amplified Spontaneous Emission (ASE) pre-lasing between the rod and 100% mirror when the flashlamp energy was increased above 25 Joule. At this level, 80% of shots were SLM but only contained 20mJ of energy. With the Pockels cell and polariser between the rod and 100% mirror, 45mJ pulses could be obtained before ASE pre-lasing occurs. This time we were troubled by spatial hole burning (see next section) which could have been eliminated by placing $\lambda/4$ plates around the rod. Even so, we are nowhere near the desired 100mJ output which was the limit when operating fast Q-switched.

To sum up this section, therefore, we have shown that all three rods can be operated in a single longitudinal mode though with certain predictable limitations on the ratio of SLM to multimode shots, and, in the case of the 4.00mm rod, with some limiations on the energy output due to ASE. The next section will deal with some further improvements that can be made to the general operation of the telescopic resonator, and in particular, with refinements that allow us to improve the SLM operation to such a point that 100% of output pulses are single longitudinal mode.

2.5.3 Further Refinements to SLM Operation and the Telescopic Resonator

In determining the operation of the three rod sizes when pre-lase Q-switched it was not mentioned that there is a definite advantage to be gained by keeping the rod itself close to the end mirror. The reason for this is that it helps to minimise the effect of spatial hole burning. This effect is a result of the fact that when a resonator is oscillating on a single longitudinal mode a standing wave exists within the cavity which has nodes and antinodes within the rod. Consequently, the inversion will only be depleted at the antinodes, leaving an appreciable amount of energy still in the rod at the nodes. This inversion can be exploited by another standing wave cavity mode whose antinodes happen to overlap with the undepleted nodal regions. If the rod is in the centre of the cavity it is the adjacent cavity mode that can best exploit this remaining inversion and when the laser is pre-lase Q-switched in this configuration, the output usually consists of the main Q-switched pulse, closely followed by another pulse containing about 30% of the output energy (Sawyers, 1981). This second pulse is separated from the first by a time which varies from shot to shot, often being close enough to partially overlap and beat with it. Placing the rod close enough to the end mirror greatly reduces this effect but a second pulse is usually still detectable. It will be almost totally eliminated however, by the placing of two quarter-wave plates around the rod (Evtuhov and Siegman, 1965). This results in the formation of a standing helical wave within the rod which has no nodes.

Consequently no inversion is left behind after the pulse due to the dominant longitudinal mode has finished.

The most significant improvement, however, in the operation of the pre-lase Q-switched telescope resonator is that SLM operation can now be achieved on 100% of output pulses. The pre-lase Q-switching technique already utilises a PIN photodiode to monitor the slow build-up of radiation within the cavity. If the signal from this photodiode is electronically monitored for the presence of adjacent mode beating it should be possible to derive from it a trigger to introduce some form of corrective measure if beating is present. One such measure is to increase the cavity length by a quarter of a wavelength by either moving a wedge across the cavity by an appropriate distance (Berry, 1982); by moving one of the end mirrors on a piezo- electric stack or by applying a voltage to a Pockels cell with either its x or y axes coincident with the polarisation in the cavity. All these processes work on the principle that a $\lambda/4$ increase in cavity length moves the cavity modes an optimum distance away from the case where two of them are approximately symmetrical about the peak of the frequency selection's transmission or reflection profile. One of the modes is always moved approximately to its peak, the other to some distance away. Consequently if this adjustment is made in time for the next shot, SLM operation will be assured.

Unfortunately, the output of the shot on which beating was detected still has beating on it and so the output of the laser is still not single mode every time.

A signal from the electronics could, of course, be used to prevent the Pockels cell from opening on the present shot as well as making the necessary correction for the next shot. This would result, however, in a number of output shots being completely missing.

During the course of investigating the various techniques just described, however, it was noticed that if the voltage on the Pockells cell was decreased a little below the optimum value for pre-lase Q-switching, and not triggered off, then a train of four or five relaxation oscillations would be obtained. One of these pulses would always be SLM. This can be explained on the basis of the cavity length being swept anyway due to the heating within the rod. If, therefore, the electronic circuit monitors each pulse in turn, it can trigger the Pockels cell open only upon detection of an SLM pulse i.e. when beating is seen to be absent during the pre-lase. In this way, therefore, every single output pulse from a pre-lase Q-switched telescopic resonator can be obtained in an SLM mode. This technique has been used successfully and is presented in more detail in Hanna and Koo (1982).

3. THEORY OF STIMULATED RAMAN AND BRILLOUIN SCATTERING

As mentioned in chapter 1 there is much interest in producing laser sources, particularly tunable ones, in the infra-red part of the spectrum. A convenient way of achieving this is to take a laser operating in or around the visible region and shift the wavelength of its output into the infrared by the nonlinear optical process known as Stimulated Raman Scattering (SRS). General analyses and applications of the SRS process have been presented by many authors (see next subsection for references) and so we shall not develop the theory in detail from first principles here, but quickly proceed to well established results such as expressions for Raman gain for plane-wave pumping. We also draw on results previously reported for Raman gain using focussed Gaussian beams (Cotter et al, 1975). In addition, since Stimulated Brillouin Scattering (SBS) can be an unwanted competing process, a similar analysis is applied to it and expressions derived for its gain and threshold powers. This, then, enables us to examine the conditions under which SRS or SBS is the dominant process. Departures from the steady-state condition will be considered, bearing in mind that under certain conditions the pump pulse lengths can be comparable to the response times of the medium. All this leaves us in a position to make threshold predictions for certain simple, single-pass Raman and Brillouin experiments. Details are given of these numerical calculations, showing how the various parameters are either derived or estimated.

One technique employed to lower the threshold powers is to form a resonator for the generated Stokes radiation. In this way the effective interaction length is increased and thus a lower pump power is required. The chapter is concluded by an extension of the theory to handle this situation.

3.1 The Plane Wave Raman and Brillouin Gain Coefficients

Raman and Brillouin scattering are both examples of inelastic scattering processes in which an incident photon of energy $\hbar w_p$ is scattered into a photon with a lower energy $\hbar w_s$. The difference in energy is always equal to some excitation quantum of the medium in which the scattering takes place. In this work the molecules of hydrogen and methane gas are excited from the ground state to the first vibrational state. Other examples of Raman scattering include rotational Raman Scattering (e.g. Trutna and Byer, 1980), where molecules are excited from the ground state to the next rotational state, and electronic Raman Scattering (e.g. Hanna, Yuratich Cotter (1979), Chapter 5) where the atom undergoes a transition to an excited electronic level. Both Raman and Brillouin scattering are examples of interactions that are nonlinear in the electric field E. The general theory has been presented by many authors e.g. Armstrong et al (1962), Bloembergen (1965) and Butcher (1965). The following brief outline is derived mainly from the work of Butcher.

Because the number of light photons involved is very large it is appropriate to represent the radiation in the form of a classical electric field. It is then possible to write the total electromagnetic field as a superposition of mono-chromatic waves;

$$E(r,t) = \int_{-\infty}^{\infty} dw\underline{E}(w)\exp(-iwt) \qquad 3.1$$

The induced time-dependent polarisation in the nonlinear medium can be written down generally as a power series;

$$\underline{P}(t) = \underline{P}^{(1)}(t) + \underline{P}^{(2)}(t)+.....+ \underline{P}^{(r)}(t)+..... \qquad 3.2$$

This is the constitutive relation where $P^{(r)}(t)$ is to the r'th power in $E(t)$. In fact, using equation 3.1 each component in equation 3.2 can be written in the form;

$$\underline{P}^{(r)}(t) = \int_{-\infty}^{\infty} dw_1 \ldots\ldots \int_{-\infty}^{\infty} dw_r \chi^{(r)}(w_1 \ldots w_r) E(w_1) \ldots E(w_r) \cdot \exp\left[it \sum_{m=1}^{r} w_r \right] \quad 3.3$$

Where $\chi^{(r)}(w_1 \ldots w_r)$ is the r'th order susceptibility, for which the general result is a rather complex summation over contributing dipole moments which depends, in particular, on the relative values of the frequencies w_n involved and transition frequencies within the medium. The nonlinear susceptibilities generally decrease rapidly in value as the order r increases. However, because of the large E values obtainable from lasers and the large values of $\chi^{(r)}$ which arise where particular frequencies coincide with transition frequencies withinthe medium, large values of $P^{(r)}(t)$ can be obtained even for high orders. Whenever there is a time varying polarisation in a medium it will radiate an electromagnetic field, the form of which can be determined by solving Maxwells equations. These yield the following wave equation;

$$\text{Curl}(\text{Curl}\underline{E}) = -\mu_o \frac{\partial^2 \underline{D}}{\partial t^2} \quad 3.6$$

Where;

$$\underline{D} = \epsilon_o \underline{E} + \underline{P}^L + \underline{P}_{NL} \quad 3.7$$

and where the nonlinear polarisation $\underline{P}_{NL}$ has been kept separate from the linear polarisation $\underline{P}^L$. We must now take account of the spatial characteristics of $\underline{E}(t)$ and write it as $\underline{E}(\underline{r},t)$.

To derive the plane-wave coefficients we assume that $\underline{E}(\underline{r},t)$ is a plane-wave propagating along the z-axis and also that it is composed of a superposition of running waves each of which is characterised by a wave-vector $\underline{k}_w = k_w \hat{\underline{z}}$ ie,

$$E(z,w) = \tilde{E}(z,w)\, e^{\pm ik_w z} \qquad 3.8$$

where $\tilde{E}(z,w)$ is a slowly varying envelope function which allows us to ignore its second derivative. Under these plane-wave approximations equations 3.6 and 3.7 then give;

$$\frac{dE}{dZ}(z,w) = \frac{iw}{2\epsilon_o c n_w} P^{NL}(z,w)\, e^{\pm ik_w Z} \qquad 3.9$$

Where w is the frequency of the field $E(z,w)$, n_w is the refractive index of the medium at this frequency, c is the velocity of light and ϵ_o is the permitivity of free space.

Equation 3.9 is the starting point for most plane-wave calculations in nonlinear optics. It represents an infinite set of coupled equations for the $E(z,w)$ since we have shown in the preceeding pages that $P^{NL}(z,w)$ is nonlinear in these fields. Solutions are obtained by restricting interest to just a few fields and assuming that these fields are monochromatic i.e. $E(z,w)$ becomes $E_w(z)$, for example. Similarly, the time dependent polarisations $P^{(r)}(t)$ can also be transformed into the frequency domain and written as the sum of a few terms of the form $P^{NL}(z,w)$ which include the susceptibilities $X^{(r)}(W_1 \ldots W_r)$.

At this point we shall restrict our attention to just Raman and Brillouin scattering instead of a completely general non-linear process considered so far. Both are examples of a third order susceptibility, resulting in a polarisation;

$$P_S^{(3)} = \frac{3}{2} \epsilon_o \chi^{(3)} | E_p |^2 | E_s | \qquad 3.10$$

Interest is being restricted, therefore, to just two monochromatic waves at frequencies w_p and w_s. In addition to this we assume at this point that only one nonlinear polarisation is relevant under any one set of experimental conditions, all others being either non-existent or negligable by comparison. With these assumptions, substituting equation 3.10 into equation 3.9 gives us two coupled equations, one for $E_p(z)$ and the other for $E_S(z)$. These can be solved simultaneously to take account of pump depletion (e.g. Von der Linde, Maier, Kaiser, 1969). Normally, however, we are interested in the small signal gain up to the threshold condition where the wave at w_3 is just detectable. In this case pump depletion is negligable and we can make the approximation $E_p(z) = E_p(0) = E_{po}$, a constant. So equation 3.9 just gives us one equation for E_s;

$$\frac{dE_S}{dZ}(z) = \frac{3iw_s}{2\epsilon_o c n_s} \cdot \chi^{(3)} \cdot E_{po}^2 E_S(z) \qquad 3.11$$

It only remains to integrate over an interaction length L. For SRS this can be done in either direction depending on whether we are considering forwards or backwards scattering. For SBS, however, it must be done for E_S travelling in the backwards direction since this direction has the maximum gain due to the dispersion characteristics of acoustic phonons. The results, however, are both the same for lossless media;

$$E_S(L) = E_{S0} \exp \left\{ \frac{3iw_S}{2\epsilon_o c^2 n_S n_P} \chi^{(3)} I_{po} L \right\} \qquad 3.12$$

where E_{S0} is starting noise at the beginning of the integration path and I_{po} is the pump intensity. Converting to intensities we get the final result;

$$I_S(L) = I_{S0} \exp(g I_{po} L) \qquad 3.13$$

$$\text{where} \quad g = \frac{-3w_S}{\epsilon_o c^2 n_S n_P} \cdot \chi^{(3)''} \qquad 3.14$$

g is the plane wave Raman or Brillouin gain coefficient. $\chi^{(3)''}$ is the imaginary part of the 3rd order nonlinear susceptibility. The real part (if there is one) would be respoonsible for a nonlinear change in the refractive index of the medium.

Equation 3.13 shows that the Stokes waves grow exponentially up to the threshold condition. Typically we require I_{S0} to grow by a factor of exp(30) to reach a detectable level, and so if we know $\chi^{(3)''}$ we can predict the threshold intensity I_{P0} required.

So numerical values for the $\chi^{(3)''}$ of Raman and Brillouin scattering must be derived. In principle this can be done by summing over dipole moment matrix elements as mentioned earlier. This can be done for simple electronic transitions in the case of Stimulated Electronic Raman Scattering in, say, caesuim vapour (see, for example; Hanna, Yuratich, Cotter, 1979). In hydrogen and Methane molecules, however, where the transition in question is between vibrational levels and where there are a large number of intermediate levels to consider this is a very complex calculation. So, for Raman scattering a different approach is often taken. An alternative definition is provided by (Hanna, Yuratich, Cotter, (1979));

$$\chi_R = \frac{N/6\hbar E_o}{\Omega_{fg} + w_S - w_p + i\Gamma} \cdot \left| \alpha_R \right|^2 \qquad 3.15$$

Here, all the matrix elements and summations that are relevant are contained in the polarisability α_R. Ω_{fg} is the vibrational transition frequency and Γ its half-width at half maximum. The polarisability can be shown to be related to the easily measurable differential scattering cross-section $d\sigma/d\Omega$ by the relation (Hanna et al 1979);

$$\frac{d\sigma}{d\Omega} = \frac{w_S^3 w_p}{(4\pi\epsilon_o c^2)^2} \cdot \left| \alpha_R \right|^2 \qquad 3.16$$

Thus, combining equations 3.16, 3.15 and 3.14 we obtain, on resonance;

$$g_R = \left(\frac{8\pi^2 c^2}{\hbar n_S n_P w_S^2 w_p} \right) \cdot \frac{N}{\Gamma} \cdot \frac{d\sigma}{d\Omega} \qquad 3.17$$

This is our final expression for the plane-wave Raman gain coefficient.

The steady state Brillouin gain coefficient can be written as (Minck, Hagenlocker, Rado, 1967; Kaiser and Maier, 1972)

$$g_B = \frac{w_S w_B T_B \left[\rho \partial\epsilon/\partial\rho\right]^2}{2V^2 n^2 c^2 \rho} = \frac{w_S^2 T_B \left[\rho \partial\epsilon/\partial\rho\right]^2}{c^3 n V \rho}$$

Where V is the acoustic phonon velocity, ρ the density, $\partial\epsilon/\partial\rho$ is the change in permittivity due to density fluctuations. T_B is the phonon lifetime and w_B the frequency of the phonon and therefore of the Brillouin shift. Often $V^2\rho$ is written as the Bulk Modulus. It can be seen that $g_B \alpha w_B$. Now $w_B = K_a V$ where K_a is the wavevector of the phonon. In a Brillouin scattering event momentum must be conserved. Since $w_P \approx w_S$ it can be shown that;

$$2 K_L \sin(\theta/2) = K_a \qquad 3.19$$

where K_L is the pump photon wave-vector and θ is the angle between pump and Stokes waves.

Clearly K_a and thus w_B and finally g_B are a maximum for $\theta = 180^o$ i.e. backwards scattering. Also clear is that the gain is zero in the forwards direction. (Note that for Raman scattering K(optical phonon) is almost independent of frequency and in any case is very small. This results in the gain being the same in all directions, forwards gain being slightly favoured by linewidth considerations, as we shall see later).

We now have workable expressions for the plane-wave gain coefficients. In sections 3.4 and 3.5 values will be found for the parameters appearing in them. But first, in section 3.2, it is necessary to relax the plane-wave approximation and develop expressions for the thresholds achievable in typical experimental arrangements.

3.2 Typical Spatial Profiles, Focussing, Gain Focussing and Diffraction

The beam from the telescopic resonator Nd:YAG laser is in the form of a circularly symmetric TEM_{oo} mode. Typically the beam would be focussed into the nonlinear medium since a high intensity is normally desirable. For an analytical treatment of the nonlinear effects produced by such beams it is necessary to go back to Maxwells equations and retain the xy dependence of the electromagnetic fields. Much of what follows is a brief summary of the theory presented in Cotter, Hanna, Wyatt (1975). The wave equation, equation 3.6, becomes

$$\nabla_T^2 E_S - 2_j K_S \frac{\partial E_S}{\partial Z} + jK_S G E_S = 0 \qquad 3.20$$

Where $G = g I_{po}, \nabla_T^2$ is the transverse component of the Laplace operator ∇^2. It is clear from our expressions for the plane-wave gain coefficients that a radial variation in the pump intensity I_{po} will result in a corresponding variation in the Raman or Brillouin gains. For a TEM_{oo} beam we should insert a Gaussian intensity profile into equation 3.20 via our expressions for G. Unfortunately, this results in an equation which can only be solved numerically. Cotter et al show, however, that the approximation;

$$G = G_o \exp(-2r^2/W_p^2) \approx G_o(1 - 2r^2/W_p^2) \qquad 3.21$$

will give analytical results agreeing quite closely with the numerical calculations. W_p is the TEM_{oo} mode spotsize and $r^2 = x^2 + y^2$. Beginning with a beam for which W_p is assumed not to change over the whole interaction length, Cotter et al employ Kogelnic's (1975) concept of a matched mode. This is a generated Stokes mode whose beam parameters remain fixed throughout the medium. Implicitly assumed in this approach is the idea that gain focussing and diffraction counteract each other so as to produce a beam of constant spotsize. Diffraction losses do still occur but the Stokes beam still experiences a net gain (albeit a reduced one when compared to the plane-wave case). The result obtained is as follows;

$$I_S(L) = I_{SO} \exp\left\{ \frac{(\tilde{P}_p - 2\sqrt{\tilde{P}_p})L}{K_S W_P^2} \right\} \qquad 3.22$$

Where $\tilde{P}_p = G_0 K_S W_p^2$ is a dimensionless quantity proportional to the pump power P_p as well as the plane-wave gain coefficient. Comparing this equation with the plane-wave equivalent, equation 3.13, it is clear that the gain focussing and diffraction introduced by confining the pump to a realistic spatial profile has lowered the gain via the additional term $-2\sqrt{\tilde{P}_p}$. Clearly this will raise the threshold power required.

The theory is extended to take account of focussing of the pump by introducing a z-dependent pump spotsize $W_p(Z)$;

i.e. $$W_p(z) = W_{po} \ (1 + \mathcal{Z})^{\frac{1}{2}} \qquad 3.23$$

where $$\mathcal{Z} = 2(Z - Z_f)/b_p$$

b_p is the confocal parameter of the beam and z_f is the position of the focus. The matched mode theory must be extended in a more generalised way and only the result is quoted here.

$$I_S(L) = I_{SO} \ \exp \left\{ \frac{\tilde{P}_p - 2\sqrt{\tilde{P}})}{K} \cdot \arctan\left(\frac{L}{b_p}\right) \right\} \qquad 3.24$$

Where $K = K_s/K_p$ and the pump is focussed into the centre of a gain medium of length L.

Rearranging this equation gives us our final expression for the pump power P_{pth} required to reach threshold in a single pass through a gain medium using a focussed TEM_{oo} mode beam;

$$P_{pth} = \frac{\pi C W_S \left[1+\left\{1+ (K/\tan^{-1}(L/b_p)).\ln(P_S(L)/P_{S0})\right\}^{\frac{1}{2}}\right]^2}{2K^2 g W_p^2} \qquad 3.25$$

As mentioned earlier, $\ln(P_S(L)/P_{S0})$ is usually set to $\sim$30 for typical detector thresholds. It must be remembered that this equation only applies for steady-state Raman and Brillouin scattering where the pump pulse duration is longer than the relevant response time of the medium.

3.3 Temporal Characteristics of Stimulated Raman and Brillouin Scattering

The dependence of the Raman and Brillouin gains on the temporal characteristics of the pump beam has been considered by many authors elsewhere e.g. Park and Byer (1979) (and references therein) but more recently by Berry and Hanna (1983) in a paper presented in Appendix II. Very simply, temporal structure in the pump pulse cannot be shorter than $\sim 1/\Delta\nu_L$, where $\Delta\nu_L$ is the linewidth of the laser. If this structure is long in duration compared to the characteristic response time of the medium ($\sim {}^{1}/_{\pi\Delta\nu_{R,B}}$) then the medium will be able to give the steady state response to any temporal variations introduced by the pump.

If, on the other hand, the duration of the structure in the pump pulse is much shorter than these response times the medium cannot respond fast enough and a transient theory must be developed to predict the new reduced gains.

An interesting consequence of this pump linewidth dependence is the variation in threshold for SRS in H_2 between a single mode, a multimode and a two-mode pump pulse, as described in the paper of appendix II. The multimode pulse has the same threshold as the single mode one because the temporal fluctuations in the former are so short that the medium cannot respond to them and so only sees the average intensity, which is the same as the single mode intensity for a pulse of the same energy and duration. The two-mode pulse, on the other hand, has variations that, as well as still being of long enough duration to be steady state, are also of higher intensity than that of a single mode pulse with the same energy. The Raman threshold energy for the two-mode pulse is therefore reduced.

A more important consequence of this temporal dependence derives from the fact that the medium response times for Brillouin and Raman scattering are quite different and depend in different ways on adjustable parameters such as the pressure. It is possible, therefore, to favour one process over the other by altering the pump pulse duration or linewidth. The best example of this is to eliminate Brillouin scattering altogether in Methane by shortening the pump pulses down to a few hundreds of picoseconds. Maintaining a fairly high pressure also helps.

Under these conditions it will be shown in future sections that Raman scattering is still in the steady state regime whilst Brillouin scattering is highly transient, and so the Brillouin gain is reduced drastically to below that of the Raman gain. As a result only Raman scattering occurs.

There are many theoretical treatments of transient Raman and Brillouin scattering in the literature e.g. Akhmanov et al (1971) and (1974). Most treat pump and stokes as step functions and consider only the case of large gains. The results are usually expressed as a modified, transient gain coefficient which can be written as;

$$G_T = 2\left(\frac{Gt}{T}\right)^{\frac{1}{2}} - \frac{t}{T} \qquad 3.26$$

Where t is the pump duration, T is the characteristic response of the medium and $G = gI_p l$. Again, we require $G_T \approx 30$ for threshold.

3.4 Numerical Predictions from Theory: Raman Scattering in Hydrogen and Methane

We are now in a position to make some predictions from theory of typical Raman thresholds expected using typical experimental arrangements. We require a value for the plane-wave Raman gain coefficient g_R. This is given by equation 3.20 and can be written as;

$$g_R = \frac{2w_S \chi_R''}{n_s n_p c^2 \epsilon_o} \qquad 3.27$$

Where;

$$\chi_R'' = \left(\frac{(2\pi)^3 n_o c^4 \epsilon_o}{\pi n_S w_P w_S^3 \hbar} \right) \cdot \frac{\Delta N}{\Delta w_R} \cdot \frac{d\sigma}{d\Omega} \qquad 3.28$$

Δ is now the full width at half maximum of the Raman transition. It is often stated that $g_R \propto 1/\lambda_S$ is the wavelength dependence of the Raman gain. This is seen to be approximately true if we recall that $d\sigma/d\Omega$ is to a first approximation proportional to w_S^4 and $w_P \approx w_S$. We must be more accurate, however, and obtain as good an estimate as we possibly can for g_R. We must also consider the pressure variation of some of the parameters. In particular, we must obtain values for ΔN, Δw_R and $d\sigma/d\Omega$. All the other terms are constants once the medium and pump wavelengths have been fixed (we ignore slight pressure variations in n_P and n_S and set each to unity).

3.4.1 Obtaining Values for ΔN, Δw_R and $d\sigma/d\Omega$

Since the differential scattering cross-section is defined as though all the molecules present are involved in the nonlinear interactions, ΔN is just the number of molecules per unit volume. This is given, to less than 2% error even at the highest pressures, by the Ideal Gas Law. We must also take into account, however, the fact that all the molecules might not be in the relevant ground state at room temperature. In general, therefore, we can write;

$$\Delta N = F \times P/kT \qquad 3.29$$

Where for hydrgoen $F = 0.66$ is the fraction of molecules in the $V = 0$, $J = 1$ ground state, and for methane, $F = 1$ since all ground state levels are used. P is the pressure (Nm^{-2}), T the temperature and k is Boltzmann's constant.

The Raman linewidth Δw_R, depends in a more complex way on the pressure. For hydrogen the linewidth of the $V = 0$, $J = 1$ to $V = 1$, $J = 1$ vibrational transition is Doppler limited below about a few hundred torr. The linewidth therefore depends on the thermal velocities of the molecules and on the relative directions of pump and Stokes beams. The linewidth is given by (e.g. Murray and Javan 1972);

$$\Delta w(FWHM) = 2K_o\sqrt{\frac{2kT\ln 2}{M}} \qquad 3.30$$

$$\text{where; } |K_o|^2 = 2K_pK_S(1 - \cos\theta) + (K_p - K_S)^2 \qquad 3.31$$

M is the mass of a molecule and θ is the angle between pump and Stokes beams. Note that there is a substantial difference between forward Stokes $K_o = K_P - K_S$ and backwards $K_o = K_P + K_S$ which is a factor of $(W_P + W_S)/(W_P - W_S)$ times bigger.

For hydrogen, using a 1.064 μm pump resulting in 1st Stokes at 1.907μm, the forwards Doppler linewidth is 0.036 cm^{-1} and the backwards linewidth is 0.127cm^{-1}. The forwards Raman gain is therefore going to be much larger than the backwards gain at these low pressures. As the pressure is increased, however, from a few hundred torr to a few atmospheres the mean free path of the molecules decreases until it becomes comparable to the wavelength of the emitted Stokes radiation.

Under these conditions molecular collisions are happening so fast that the Doppler effect can progressively see only the average velocity of the molecules, which is zero. As a result the linewidth is dramatically narrowed. This effect is known as Dicke or motional narrowing, fuller accounts of which are given by Dicke (1953) and Galatry (1961). As the pressure is raised further, however, the normal pressure broadening effect dominates. Neglecting the pressure dependence at very low pressures the Raman linewidths in hydrogen can be described by the equation (Murray and Javan, 1972);

$$\Delta w(\text{FWHM}) = \frac{D_0 K_0^{\,2}}{c\pi d} + ad \qquad 3.32$$

Where D_o is the self-diffusion coefficient found by the same authors to be $1.361/c\ cm^2$ Amagat, d is the density in Amagat units and a is the pressure broadening coefficient given by Trutna and Byer (1980) as $1.267 \times 10^{-3}\ cm^{-1}$ $Amagat^{-1}$. The first term obviously corresponds to the Dicke narrowing effect, the second the pressure broadening.

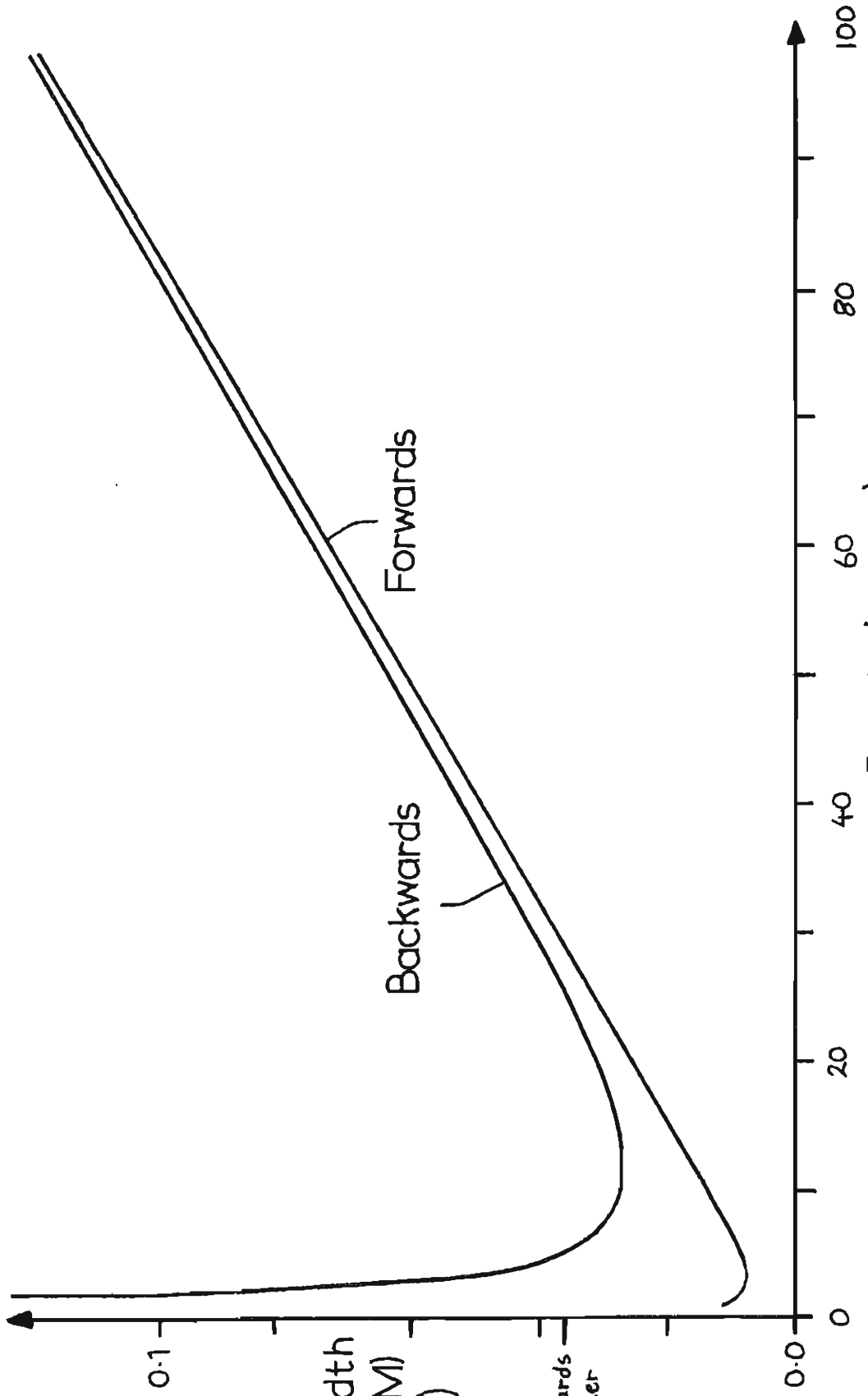

Figure 3.1: Raman linewidths for hydrogen calculated using equation 3.22.

Fig. 3.1 shows the linewidths derived from this equation, both forwards and backwards.

For Methane, which is a heavier molecule, the Doppler widths are smaller. Using the same pump, $\Delta w(\text{Forward}) \simeq 0.009\ cm^{-1}$ and $\Delta w(\text{backwards}) \simeq 0.05 cm^{-1}$. The vibrational transition involved actually contains a number of different rotational levels which, because of the narrow forwards Doppler width, can be resolved at low pressures (May et al, 1978). However, pressure broadening becomes significant at around 1 atmosphere before Dicke narrowing can have any effect, and by about 3 atmospheres the rotational levels have all been smeared out into a single, nearly symmetrical Lorentzian. At higher pressures this continues to be broadened in the normal way. Taira et al (1982) have measured the linewidth in the region 3-50 Atm. They obtain for the forwards linewith;

$$\Delta w_R = 0.32 + 0.012.P \quad cm^{-1} \qquad 3.33$$

where P is the pressure in atmospheres. The backwards linewidth is the same as the forwards above about 10 Atm, below this residual Doppler effects make it larger than the forwards one.

The differential scattering cross-sections $d\sigma/d\Omega$ are calculated from tabulated measurements taken at other wavelengths.

These in turn are usually quoted as some factor times a standard measurement, normally that of scattering in nitrogen. Fenner, Hyatt, Kellam and Porto (1973) give values for $d\sigma/d\Omega$ for H_2 and CH_4 using 514nm radiation.

$$H_2 \text{ (all transitions)} \quad ; \quad d\sigma/d\Omega = 2.2 \times 4.3 \times 10^{-31} \text{ cm}^2/\text{sr}$$
$$CH_4 \text{ (all transitions)} \quad ; \quad d\sigma/d\Omega = 6.0 \times 4.3 \times 10^{-31} \text{ cm}^2/\text{sr}$$

We have seen that for H_2 the factor of $0.66 \ln \Delta N$ ensures that we only consider the $V = 0, J = 1$ to $V = 1, J = 1$ transistion. Schotter and Klockner (1979) describe how these cross-sections are corrected for use at different pump wavelengths. The relevant equation is;

$$\left.\frac{d\sigma}{d\Omega}\right|_{\lambda p} = \frac{W_S^{\,4}(\lambda_p)}{W_S^{\,4}(\lambda_p = 514\text{nm})} \cdot \frac{\left(\frac{1}{\Omega_{1g} - W_p} + \frac{1}{\Omega_{1g} + W_S}\right)^2_{\lambda p}}{\left(\frac{1}{\Omega_{1g} - W_p} + \frac{1}{\Omega_{1g} + W_S}\right)^2_{\lambda p = 514\text{nm}}} \cdot \left.\frac{d\sigma}{d\Omega}\right|_{\lambda p = 514\text{nm}} \qquad 3.34$$

The first term is the normal $W_S^{\,4}$ frequency dependence. The second term takes into account the dispersion due to the intermediate level. In hydrogen this is at $\Omega_{1g} \approx 90{,}000 \text{ cm}^{-1}$. 514nm is the most common wavelength at which cross-sections are measured. The estimated errors on the cross-sections are about $\pm$ 20%. Trutna and Byer (1980) give no indication of the possible error on the pressure broadening coefficient a, but Murray and Javan (1972) claim errors of less than 7% on similar measurements. Combining this with the few percent error on the number density gives us a possible error of about 30% in the plane-wave gain coefficient. The analysis of Cotter et al (1975), for predicting actual threshold values will introduce a further few percent error and so the overall error is still around 30%.

3.4.2 Calculated Threshold Powers

The predicted pump thresholds for a number of pump wavelengths will be worked out for hydrogen gas at 30 atmospheres pressure. 30 atmospheres is chosen because at this pressure the linewidth is well into the pressure broadened regime resulting in maximum gain. In each case fairly tight focussing of the pump beam is used, the actual value of L/b_p used being taken from experiments described in the next chapter. The population density of equation 3.29, the linewidth from equation 3.32 and the differential scattering cross section of equation 3.34 are all substituted into equations 3.27 and3.28 to give the plane-wave coefficients. These are then substituted into equation 3.25, with the relevant focussing values, to give us our predictions for the Raman threshold powers. The results are presented in the table below.

Table 3.1 Predicted threshold powers for unguided SRS in H_2

Pump Wavelengths (μm)	1.650	1.064	0.532	0.355	0.266
1st Stokes Wavelengths (μm)	5.23	1.907	0.683	0.416	0.299
Plane wave gain coeff. (cm/GW)	0.14	0.69	2.86	5.74	9.90
Focussing: L/b_p	15	10	3	13	10
Threshold power (kW)	12778	1370	175	50	22

The Raman shift in hydrogen is $4155.2cm^{-1}$, the largest shift available from a simple vibrational transition. The wavelengths chosen are the Nd:YAG fundamental, its harmonics and 1.65μm - a typical wavelength from a low power F-centre or vibronic laser. Clearly, the threshold powers are rather high for the longer wavelengths. This is one of the reasons for which the wave-guide techniques described in this thesis were investigated. We shall see that their use drastically reduces these predicted threshold powers.

For methane we anticipate the fact that for the longer wavelengths (532nm and above) the Brillouin gain will be larger than the steady state plane-wave Raman gain and so Raman scattering will not occur with our 30ns long pre-lase Q-switched pulses. With pulse lengths that are 100-500ps long, however, it can be shown using the arguments of the previous section that the Raman effect remains in the steady-state regime whilst the Brillouin effect becomes transient, resulting in much higher thresholds. Although a high power, short pulse, multi-wavelength source was not available in the laboratory, the predicted results are presented below for comparision with hydrogen, and also because the gain coefficients will be needed in future chapters. The pressure was kept at 30 Atm. for a direct comparison. The results were calculated in the same way as the hydrogen results.

Table 3.2 Predicted threshold powers for unguided SRS in CH_4

Pump Wavelengths (μm)	1.65	1.064	0.532	0.35	0.266
1st Stokes Wavelengths (μm)	3.169	1.544	0.629	0.396	0.288
Plane Wave gain Coeff (cm/GW)	0.068	0.185	0.555	0.936	1.323
Focussing: L/b_p	15	10	11.5	13	10
Threshold Power (kW)	22310	4958	781	303	162

The Raman shift in methane responsible for the 1st Stokes wavelengths presented is $2916cm^{-1}$. It can be seen that the gain coefficients are substantially lower than those for hydrogen, largely due to the bigger Raman linewidths given by equation 3.33.

3.5 Numerical Predictions from Theory: Brillouin Scattering in Hydrogen and Methane

To make predictions of the expected Brillouin scattering pump threshold powers we again need a value for the plane-wave gain coefficient, this time given by equation 3.18 as;

$$g_B = \frac{w_S^2 T_B [\rho \partial \epsilon / \partial \rho]^2}{c^3 n V \rho} \qquad 3.18$$

Minck, Hagenlocker and Rado (1967) obtain numerical values for hydrogen at various pressures, but at the low temperature of 77K.

Lowering the temperature greatly increases the Brillouin gain coefficients. At room temperature and typical pressures chosen for Raman scattering the Brillouin gain is much less than the Raman gain in hydrogen and so Brillouin scattering never occurs - certainly it has never been a problem in any experiments performed in the work for this thesis. Methane, on the other hand, has comparable experimental Raman and Brillouin gains at ordinary temperatures and pressures, and so an attempt will be made to derive the predicted Brillouin gain coefficient.

3.5.1 Obtaining Values for the Parameters in the Gain Coefficient

The frequency shift resulting from Brillouin scattering is given by $w_B = 2K_L V$. Since the velocity of sound V is very small compared to the velocity of light c, $W_B \ll W_p$ and So $W_s \approx W_p$ in equation 3.19. Again the refractive index n is put to unity. The quantities of interest are therefore the phonon lifetime T_B, the coefficient of electrostriction $[\rho \partial\epsilon / \partial\rho]$, the acoustic phonon velocity V and the density ρ.

An expression for the phonon lifetime (Dr J G Hey, private communication) can be written as,

$$T_B = \frac{\rho}{4K_L^2 \left\{ \eta(T) + K(T) \left[\frac{1}{C_V(T)} - \frac{1}{C_P(T)} \right] \right\}} \qquad 3.35$$

Where $\eta(T)$ is the viscosity, $K(T)$ the thermal conductivity and $C_P(T)$, $C_V(T)$ the specific heats at constant pressure and volume respectively. All these quantities can be obtained from standard tables.

An expression for $\left[\rho\, \partial\epsilon/\partial\rho\right]$ can be obtained by differentiating the Clausius-Mossotti equation for non-polar gases with respect to the density ρ. The result at a fixed pressure P is;

$$\rho \left.\frac{\partial \epsilon}{\partial \rho}\right|_P = (\epsilon_r - 1)_P \qquad 3.36$$

$\epsilon_r - 1$ can be obtained from tables. Note here that it is this quantity which is responsible for the $g_B \propto P^2$ dependence of the Brillouin gain. The acoustic phonon velocity is just the speed of sound in methane and can also be obtained from tables. The density can be calculated from the pressure using the Ideal Gas Law. This quantity is needed only for the phonon lifetime values since it cancels out if equation 3.35 is substituted in equation 3.18. The result of doing this can be written as (including equation 3.36);

$$g_B = \frac{(\epsilon_r - 1)^2}{4cV(T)\left\{\eta(T) + K(T)\left[\frac{1}{C_V(T)} - \frac{1}{C_P(T)}\right]\right\}} \qquad 3.57$$

This is our final expression for the steady-state Brillouin gain. Normally this number would be evaluated and substituted into equation 3.25 to determine the threshold pump power under realistic focussing conditions. We are assuming here that the same matched mode analysis applies for Brillouin scattering as for Raman scattering.

Anticipating differences between predicted and experimentally measured thresholds it is worth noting here that Trutna and Byer (1980) derive a different expression from Cotter et al for the threshold powers using focussed Gaussian beams (see next section). Their expression is;

$$P_{p,th} = \frac{2\lambda_p \ln(P_S/P_{S0})}{4g \tan^{-1}(L/b_p)} \qquad 3.58$$

where again we have assumed that $\lambda_p \approx \lambda_s$.

Another point worth anticipating is that when the numbers are put in equation 3.35 for the phonon lifetimes, it is found that they are comparable to typical pump laser pulse lengths at high pressures, and so the transient regime is being approached. To deal with this we need values for the transient gain coefficients and these are given by equation 3.26. It can be shown that if equation 3.26 is incorporated into equation 3.25 for focussed Gaussian beams, the new transient regime threshold power is given by;

$$P_{P,th} = \frac{\pi w_S c\left[1 + \left\{1 + (KT/4t \tan^{-1}\left[L/b_p\right]).\ (30 + t/T)^2\right\}^{1/2}\right]^2}{2K^2 w_p^2 g} \qquad 3.59$$

If equation 3.58 is used instead of equation 3.25 the result is;

$$P_{p,th} = \frac{2\lambda_p (T/4t)(30 + t/T)^2}{4g \tan^{-1}(L/b_p)} \qquad 3.60$$

3.5.2 Calculated Threshold Powers

The plane-wave gain coefficients will be calculated at 1 Atm and then the equation;

$$g_B(P) = g_B\ (1\ \text{Atm}).\ P^2 \qquad 3.61$$

can be used to predict the gain at any other pressure. A typical focussing parameter of $L/b_p = 1.31$ is used here as well as in the experimental measurements. The values obtained from tables for the parameters in equations 3.55 and 3.57 are as follows (all at 1 Atm);

Table 3.3 Numerical parameters used in the calculation of the SBS gain coefficient for CH_4

Parameter	Value	Units
η_s (at 293K)	1.087×10^{-5}	Ns/m^2
V (at 273K)	4.3×10^{2}	m/s
$\epsilon_r - 1$ (at 273K)	8.54×10^{-4}	
C_p (at 298.15K)	3.56×10^{1}	$JK^{-1}mol^{-1}$
K (at 300K)	3.42×10^{-2}	$J\ s^{-1}\ m^{-1}\ K^{-1}$
R (Gas constant)	8.314	$JK^{-1}\ mol^{-1}$

The results of interest are the phonon lifetime given by equation 3.35; the factor $T_B/4 \quad (30 + t/T_B)^2$ necessary for the transient equations, (we assume here that t = 30 ns, the typical pulse width from a pre-lase Q-switched telescopic resonator); the steady state threshold powers predicted by either equation 3.25 or equation 3.58 (Trutna and Byer's theory) and finally the transient theory threshold powers predicted by equation 3.59 and equation 3.60. The results are calculated at various pressures using equation 3.61 and are presented in table 3.4. All these thresholds are independent of pump wavelength insofar as we have approximated $w_S \approx w_p$ and assumed that $\epsilon_r - 1$ is frequency independent to a first approximation.

If we compare the gain coefficients of this table with those of table 3.2 for Raman scattering in methane we can see that the Brillouin gain coefficients are all much bigger. Only down at a few atmospheres pressure (where the gain coefficients of table 3.2 must be approximately halved) do they become comparable for 1.064 μm pumping. This is consistent with the fact that steady-state Raman scattering in methane gas using a 1.064 μm pump has not been reported.

The relative merits of the four sets of predicted thresholds will be considered in the next chapter where experimental results will also be presented to compare with them. Suffice it to say that the transient results are likely to be the more accurate ones since the steady-state condition $\Delta\nu_L \ll \Delta\nu_R/G$ (where the highly nonlinear dependence of Stokes growth is also considered - Ibison, 1982) gives, for a 30ns long, single mode pump pulse and an assumed G = 30 gain, $T_B \ll$ 1ns. From table 3.4 this is clearly not the case at all pressures, especially the higher ones.

P(Atm)	g_B cm/GW	T_B(ns)	$\frac{T_B}{4t}(30 + t/T_B)$	Pp(th) (MW) S-S (Eq. 3.25)	Pp(th) (MW) S-S (Eq. 3.58)	Pp(th) (MW) transient (Eq. 3.59)	Pp(th) (MW) transient (Eq. 3.60)
10	0.909	3.13	39.6	1.015	1.34	1.27	1.77
15	2.045	4.70	49.84	0.451	0.60	0.685	1.00
20	3.636	6.29	60.27	0.254	0.335	0.452	0.673
25	5.681	7.83	71.05	0.162	0.214	0.332	0.507
30	8.181	9.39	82.01	0.113	0.150	0.262	0.410
35	11.135	10.96	92.80	0.083	0.110	0.215	0.340

Table 3.4 Predicted Steady-State and transient Brillouin Scattering Threshold powers using the theories of Cotter et al and Trutna and Byer

The question then only remains of whether the Trutna and Byer expression is a better description than that of Cotter et al. Note also, however, that a fast Q-switched telescopic resonator, having a linewidth of $\sim 0{\cdot}3\ cm^{-1}$, will have temporal structure of duration ~ 0.1 ns. Compared with the phonon lifetimes of table 3.4 this is highly transient (especially with the extra G factor) and yet Raman Scattering is still around the edge of the steady-state regime. It is expected, therefore, that Raman scattering should occur before Brillouin scattering for fast Q-switched pulses - especially at lower pressures.

3.6 The Raman or Brillouin Oscillator

As mentioned in the introduction to this chapter, one method by which Raman or Brillouin thresholds can be reduced is to form a resonator for the generated Stokes radiation. This has the effect of greatly increasing the interaction length for the process and thereby reducing the pump powers required to produce the same overall net gain.

At first one might suppose that the focussed beam theory of Cotter et al (1975) could be repeatedly applied for the many cavity transits the Stokes radiation makes in the duration of the pump pulse, due account being taken of the end mirror reflectivities. That this can not be done now is largely due to the fact that there is a compromise between the tendency of gain focussing to establish a particular matched Stokes mode size, and the tendency of the resonator to establish a mode satisfying self-consistency (i.e. repeating on each round trip).

A more appropriate treatment would therefore be to take into account the amount by which the pump beam overlaps the Stokes modes of the oscillator. If the pump beam is a TEM_{oo} mode then we would expect that the best overlap would be with the TEM_{oo} mode of the resonator. Further, we would expect the minimum threshold for some matching condition where the two modes were of the same order in size.

Boyd and Kleinman (1968) and then Boyd, Johnson and Kaminow (1969) perform just such an analysis. The nonlinear susceptibilities and polarisations are defined in just the same way as in the early parts of this chapter, but they then show, again by substitution of the polarisation in Maxwells equations, that the increment in Stokes power per transit in a particular mode TEM_{mn} of a resonator is given by;

$$\Delta P_{S(m,n)} = -Im\left\{ \frac{w_s}{2} \int E^{*}_{S(m,n)} \; P_S \; dxdydz \right\} \qquad 3.62$$

P_S is the nonlinear polarisation given by (in the case of Raman and Brillouin Scattering) equation 3.10, where we take only the imaginary part of $\chi^{(3)}$. We can see from equation 3.62 that it contains an overlap integral as suggested above, $E^{*}_{S(m,n)}$ acting as a projection operator to pick out the contribution that the polarisation makes to the Stokes field $E_{S(m,n)}$. All that we need to do now is substitute in pump and Stokes fields with the appropriate spatial profiles.

We shall see in chapter 5 that this can be done for a capillary waveguide. We concentrate here on an unguided resonator. Kogelnic and Li (1966) show that stable resonators support Gaussian beams, and that for the TEM_{oo} beam in a symmetric resonator the waist size in the centre is given by;

$$W_o = \sqrt{\frac{\lambda}{2\pi}} \cdot (2Rd - d^2)^{1/4} \qquad 3.63$$

Where R is the radius of curvature of the two mirrors and d is the distance between them. Now the electric fields of focussed Gaussian beams can be written as;

$$E = \frac{E_o}{1+iT} \exp\left\{ \frac{-r^2K}{b(1+iT)} \right\} \qquad 3.64$$

Where $r = x^2 + y^2$, $K = 1/\lambda$, $T = 2z/b$ and $b = 2\pi W_o^2/\lambda$ is the confocal parameter, W_o being given by equation 3.63. If the pump beam and Stokes beam are both written in this form and substituted into equation 3.62 the result is (for $\Delta P_S/P_S \ll 1$);

$$\frac{\Delta P_S}{P_S} = \ln\left(\frac{P_S(L)}{P_S(0)}\right) = 4P_p g\, A \tan^{-1}\left(\frac{LB}{2}\right) \qquad 3.65$$

Where $A = \left[\lambda_p^2\left\{1 + (W_{SO}/W_{PO})^2\right\} + \lambda_S^2\left\{1 + (W_{PO}/W_{SO})^2\right\}\right]^{-\frac{1}{2}}$

and $B = \dfrac{1}{\pi W_{PO}^2 A\left\{1 + (W_{SO}/W_{PO})^2\right\}}$

For a fixed P_p the maximum of this function occurs when $(W_{SO}/W_{PO})=\sqrt{\lambda_S/\lambda_P}$, the equation then reduces to;

$$\ln\left(\frac{P_S(L)}{P_S(0)}\right) = \frac{4P_p g}{\lambda_p+\lambda_s} \cdot \tan^{-1}\left(\frac{L}{b_p}\right) \qquad 3.66$$

Where b_p is the confocal parameter of the pump. This is the result quoted by Trutna and Byer (1980) which they then go on to use (erroneously we feel) in a theory for their single-pass threshold measurements where $\ln (P_S(L)/P_S(0))$ is set to ~ 30.

Note that equation 3.65 contains the pump power P_p. For steady-state single pass experiments it was possible to approximate this value by the peak power occurring in a typical pulse from a Q-switched laser. Now that the Stokes is being resonated for the entire duration of the pump pulse, the temporal profile of the latter must be taken into account. For a pre-lase Q-switched pulse the profile is approximately a Gaussian and can be written as;

$$P_p(t) = P_{P0}(0) \exp(-2.773t^2/T^2) \qquad 3.67$$

where T is the full width at half maximum power. It is shown in appendix III that if a pump pulse of this form propagates in one direction only through a Stokes resonator of length L and mirror reflectivities R_1 and R_2 for the Stokes wave, the peak power P_{P0} in the pump pulse that is required to reach threshold is given by equation A7, and can be written as;

$$P_{P0} = \frac{30 - \left((n-1)/2\right)\ln(R_1R_2) - \ln(1-R_2)}{4g_F A \tan^{-1}(LB/2) \cdot S} \qquad 3.68$$

Where $S = \left[1 + 2b\exp(-at_T^2/T^2) + 2\exp(-a(2t_T)^2/T^2) \ldots + 2\exp\left(-a\left\{\frac{n-1}{2}\cdot t_T/T\right\}^2\right)\right]$

Where C in equation A7 has been replaced by $4A\tan^{-1}(LB/2)$ from equation 3.65 and the linear Stokes losses have been set to zero. t_T is the cavity transit time and $a = 2.773$. If P_p given by equation 3.68 is evaluated for an increasing number of cavity transits a minimum of P_{P0} will be found for a certain number of transits. Beyond this the cavity losses start to have more of an effect than the increased interaction length. The minimum P_{P0} will be the experimentally measured threshold power.

This is our final result for the unguided Raman or Brillouin oscillator. Equation 3.68 is best evaluated on a computer where n can be varied until a minimum of P_p is obtained. A simple programme was therefore written for this purpose. The theory was checked experimentally in a short experiment described in the next chapter. The main interest in this theory, however, occurs when it is extended to cover the case of a waveguide oscillator, as we shall see in chapter 5.

4. EXPERIMENTAL INVESTIGATIONS OF UNGUIDED RAMAN AND BRILLOUIN SCATTERING

In this chapter the theoretical predictions of chapter 3 for single-pass, tightly focussed, unguided Raman and Brillouin thresholds are compared with experimentally measured values. These measurements were made to provide a benchmark against which the performance of guided wave processes could be judged. Also, good agreement between theory and experiment was sought to give confidence both in the value of the material parameters used and in the later extension of the theory to handle guided wave situations.

In the single-pass experiments detailed below the theory was tested using different pump wavelengths, different pump linewidths and also at different hydrogen and methane gas pressures. Fairly tight focussing was used in each case since equations 3.25 or 3.59 clearly show that the lowest threshold is obtained with tight focussing. It must be remembered, however, that for the longer wavelengths, where the expected thresholds are going to be high, a limitation on tightness of focussing is imposed by the occurrence of gas breakdown. A typical intensity value for this is around 3 or 4 GW/cm^2.

In addition to the single-pass experiments a hydrogen Raman oscillator was briefly looked at as another, though much less successful, alternative to guided configurations as a method for reducing the threshold powers.

4.1 The Basic Experimental Arrangement

The experimental arrangement used for both Raman and Brillouin Scattering is shown in fig. 4.1. Very simply, the output of the telescopic resonator is passed through a variable attenuator and then focussed into a cell containing the hydrogen or methane gas. The focussing lens system is arranged such that the focussed beam waist is at the centre of the nonlinear medium. Alternatively, the output of the telescopic resonator can first be converted to its 2nd or 3rd harmonics and these used instead as the pump wavelengths. In all three cases the light emerging from the gas cell in the forwards direction is passed through a system of diagnostics where either the residual pump beam is monitored, 1st Stokes detected and measured or both. Some elements of the experiment, however, need further explanation.

4.1.1 The Telescopic Resonator

The telescopic resonator used in all the single-pass experiments comprised a 9.53 mm diameter rod with the appropriate cavity built around it, as detailed in tables 2.1 and 2.2 of chapter 2. In all cases the output was taken from the narrow beam end of the cavity which always consisted of an uncoated resonant reflector capable of handling high powers. The theory of chapter 2 and also computer performed ABCD matrix calculations predict a waist size of 0.41mm at the resonant reflector. This value is needed for all beam matching calculations.

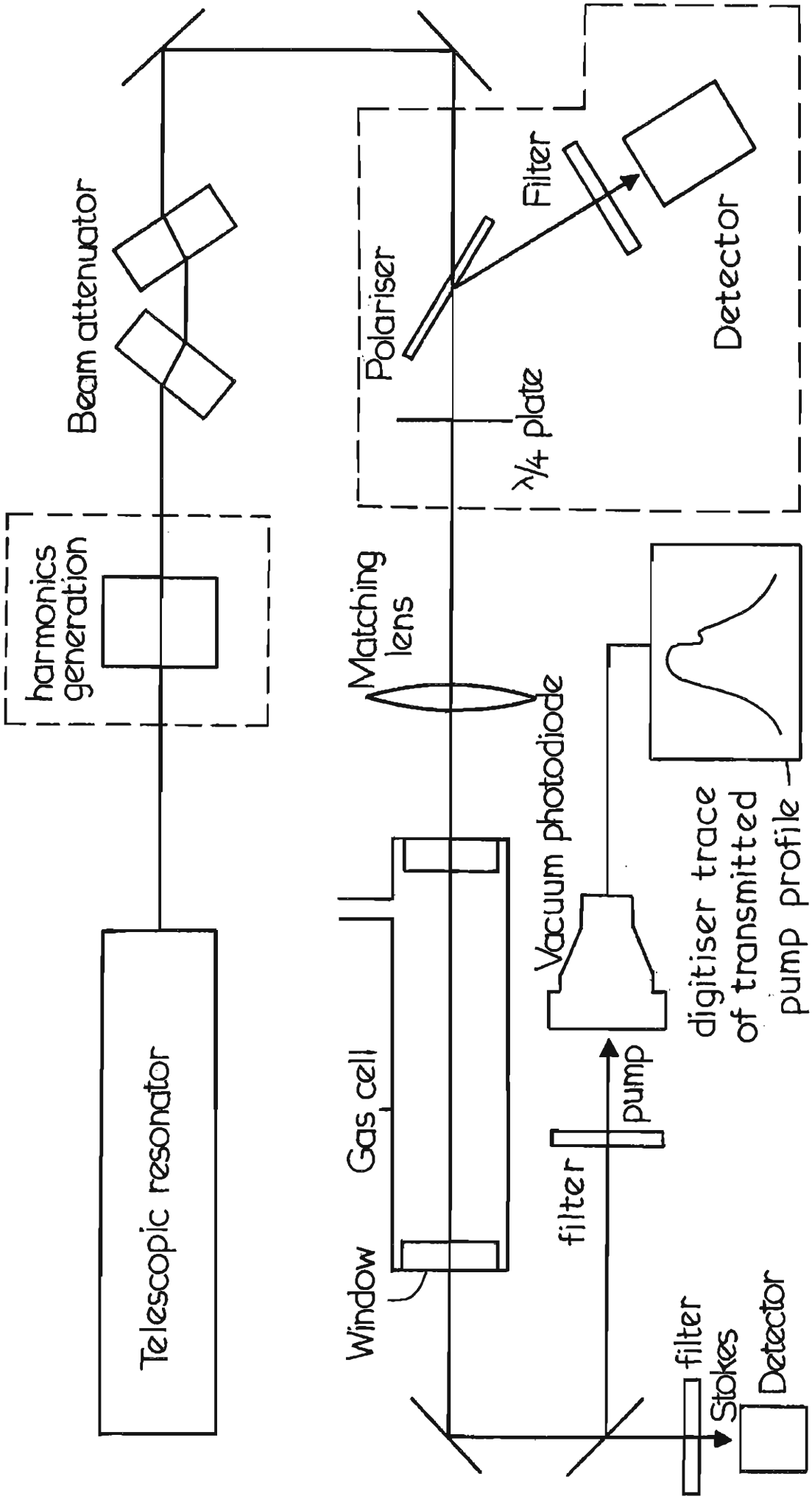

Figure 4.1: The basic experimental arrangement for single-pass Raman and Brillouin experiments.

When operating pre-lase Q-switched the mode selection was provided by a 7.5 cm long resonant reflector in conjunction with a 6mm thick, 20% reflectivity per face intra-cavity etalon, as shown in fig. 2.9, design (1). No attempt was made to temperature stabilise the mode selectors, nor was any electronic monitoring of the pre-lase build-up performed. Consequently, the output was SLM on about 80% of shots, the remaining 20% being two-mode shots of various degrees of amplitude modulation. On some shots baseline modulation was observed corresponding to beating between two modes of equal amplitude. It is these shots that were used to measure two-mode thresholds. On single mode shots, therefore, the linewidth is less than the cavity mode spacing i.e. $\Delta\nu_L < 1/2L = 0.0045$ cm^{-1}. In fact a recent measurement (I D Carr, private communication) has revealed it to be $\Delta\nu_L = 0.001$ cm^{-1}. For two mode operation $\Delta\nu_L = 0.0045$ cm^{-1}. To deliberately achieve multimode operation, ideally all mode selection should be removed and in addition fast Q-switching should be used. This would result in a linewidth of ~ 0.3 cm^{-1} due to gain narrowing alone (Equation 2.15). In our case, however, we still keep a 6mm resonant reflector as the output coupler to allow high power operation and this will result in further mode selectivity. Calculations using the equations of section 2.3.1 reveal that the linewidth will be narrowed to around 0.06 cm^{-1} and not the value of 0.3 cm^{-1} quoted in appendix II. The value of 0.06 cm^{-1} is, however, still sufficiently multimode for our purposes.

In all three cases the 100mJ output was obtained, pulse lengths being typically around 25-30ns. Amplitude stability was better than about 5%.

4.1.2 The Raman (Brillouin) Cell and Gas Handling System

Hydrogen and methane pressures up to about 50 atmospheres are of interest and so a strong, well designed gas cell and gas handling system was needed incorporating features such as over-pressure release valves and gas flushing facility. The final design arrived at is shown in fig. 4.2. Most of it is self-explanatory. The gas cell itself is constructed from standard 'Aminco' stainless-steel end tees and pipe. When the pressure is to be varied, as in most of the measurements in this chapter, it is convenient to leave the cell attached to the gas handling system. In these cases the tap and pressure gauge attached to the cell are not necessary. Of critical importance are the two end windows of the gas cell. To avoid any feedback effects the surfaces of these windows must make a large angle with the direction of the pump beam. To achieve minimum loss this angle would have to be Brewster's angle. Thus, cylindrical Brewster windows were designed, as were special bolts to hold them. These are shown in the diagram. The windows are held in place, against O-rings, by the gas pressure within the cell. The thickness of the windows (made at ICOS in Spectrosil B) was sufficient to provide a wide safety margin at 50 atmospheres pressure. They also provided a free aperture of 5mm, sufficient to allow tight focussing at the wavelengths used in cells around 50 cm long.

4.1.3 The Beam Attenuator

A technique was needed to vary the pump pulse intensity whilst leaving the pulse length and beam direction unaltered. An ability to handle a high intensity was also necessary.

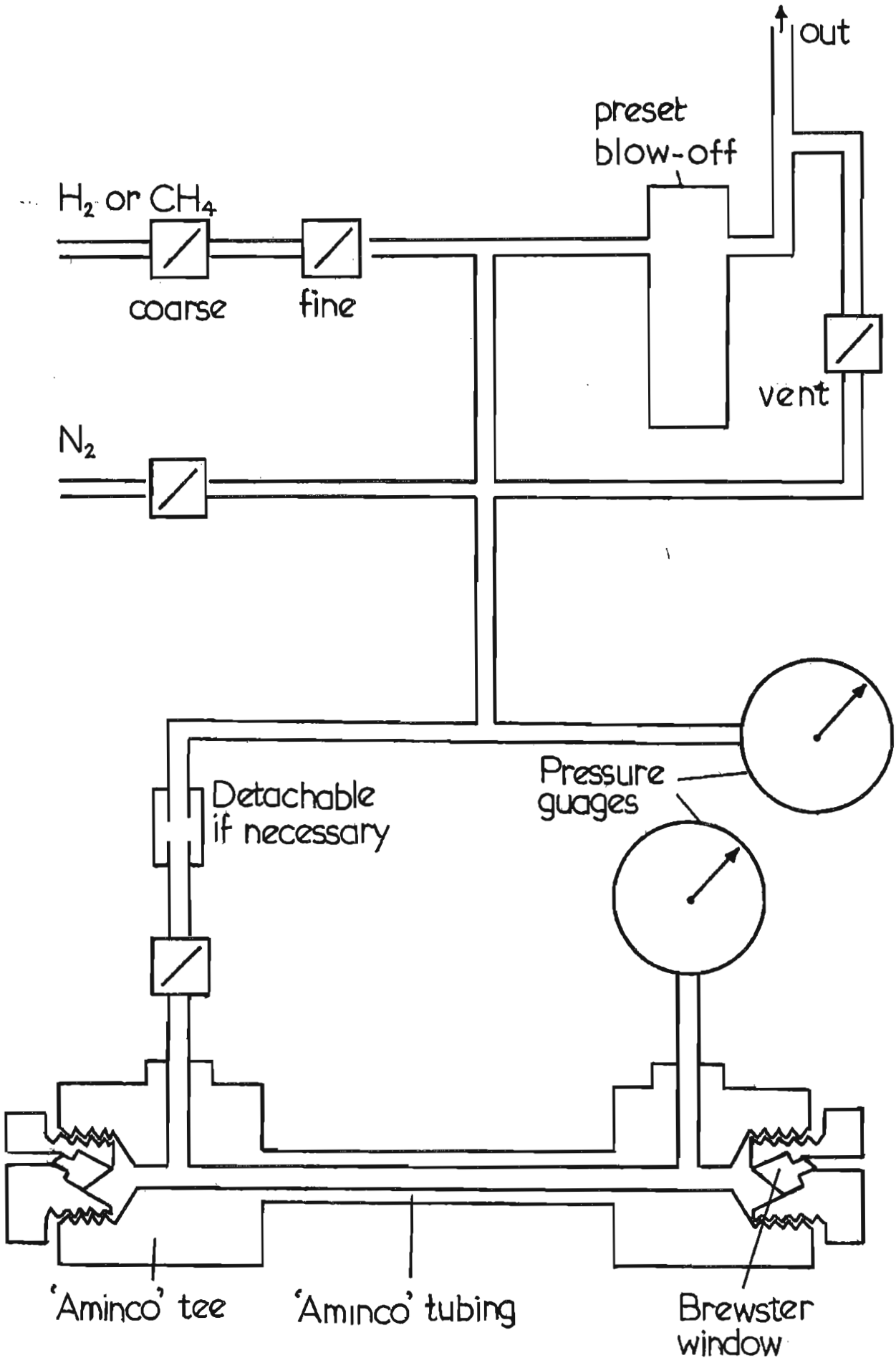

Figure 4.2: The gas cell and gas handling system.

The method employed here, and also in experiments with guided configurations, made use of two glass flats which could be set accurately at any given angle as shown in fig. 4.3. If the angle of incidence is the same for both flats, and they are both unwedged and of equal thickness, then the main beam will pass through undeviated. The plates act as a variable (polarisation dependent) attenuator because the intensities reflected and refracted at an air/glass interface depend on the angle of incidence. The larger the angle of incidence (for the S-polarisation) the greater the reflection and the less is the transmission. When all four surfaces are taken into account the total power transmission is;

$$T = \left[\frac{\mathrm{Sin}(2i)\,\mathrm{Sin}(2r)}{\mathrm{Sin}^2(i+r)\cos^2(i-r)}\right]^4 \quad \text{for p-polarisation} \qquad 4.1$$

$$T = \left[\frac{\mathrm{Sin}(2i)\,\mathrm{Sin}(2r)}{\mathrm{Sin}^2(i+r)}\right]^4 \quad \text{for s-polarisation} \qquad 4.2$$

where i is the angle of incidence and r is the angle of refraction given by $r = \mathrm{Sin}^{-1}\,(\mathrm{Sin}i/n)$, n is the refractive index of the glass.

Fig. 4.3 also shows the rejected beams that must be dealt with safely, and also extra reflected beams which must be blocked to ensure that only the beam transmitted straight through without any reflections is the one that reaches the rest of the experiment.

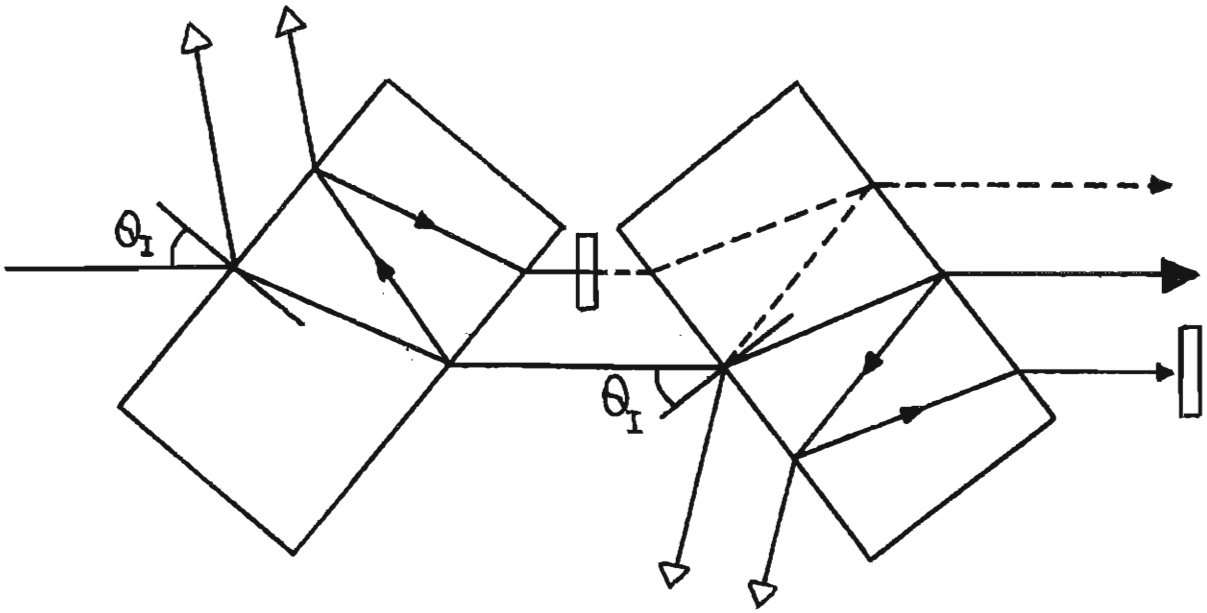

Figure 4.3: The two-plate beam attenuator showing the relevant beam paths.

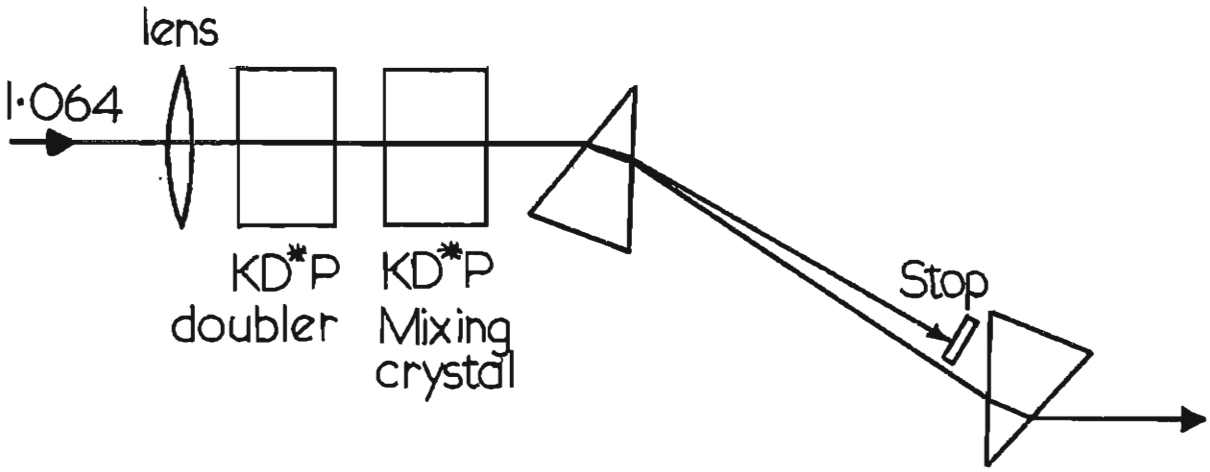

Figure 4.4: 2nd and 3rd harmonic generation.

The beam splitter is normally used such that the incident beam is s-polarised since this results in a smoothly increasing loss as the angle of incidence is increased i.e. there is no Brewster's angle for this polarisation. In addition, the losses are higher than the losses at the same angle for the p-polarisation. In the s-polarisation orientation the attenuation varies between 15% at $i = 0^{o}$ and 95% at 80^{o}.

4.1.4 2nd and 3rd Harmonic Generation

The output of the telescopic resonator at 1.064μm can be converted to its second harmonic at 532nm using a frequency doubling crystal. In our case a 2.4cm long piece of type I phase-matched KD*P was used. It was cut for critical phase matching ($\theta_m = 40.5^{o}$) and room temperature operation. The divergence of the telescopic resonator is 0.83 mRad when the output is taken from the narrow beam end ($W_o = 0.41$mm). This is comparable to the 0.67 mRad acceptance angle of the doubler (Koechner (1976)) and would result in a reduced doubling efficiency. Thus, a collimating lens was placed just before the doubler. In this case a 1m lens was used at a distance of 60cm from the telescopic resonator. This produces a waist at the exit to the lens, having a spotsize of 0.645mm. A waist makes the calculation of 2nd harmonic spotsizes and subsequent beam matching mucheasier, i.e. $W_o(532\text{nm}) = W_o(1.064\mu\text{m})/\sqrt{2}$, and it is still a waist.

The 2nd harmonic is separated from the fundamental using two prisms, (fig.4.4). Prisms have an advantage over filters in that they do not absorb energy, heat up and distort the beam; and over mirrors in that they do not have a residual transmission at the wavelength to be eliminated. The prisms can also be used at Brewster's angle if losses are an important consideration.

The 3rd harmonic is produced by including a KD*P mixing crystal immediately after the doubler. This crystal adds together a fundamental and a 2nd harmonic photon to produce a photon at the 3rd harmonic i.e. 355nm. Again a waist is desirable at the input, the resulting waist spotsize of the 3rd harmonic being given by W_o (355nm) = W_o (1.064μm)/$\sqrt{3}$.

The polarisation of the 2nd harmonic from the type 1 doubler is at 90^o to the fundamental. The type II mixing crystal resulted in a 3rd harmonic polarisation in the same plane as the fundamental.

The pulse lengths are also shortened by the nonlinear process. The relationships are analogous to the spot-size relations i.e. τ(532nm) = τ(1.064μm)/$\sqrt{2}$ and τ(355nm) = τ(1.064μm)/$\sqrt{3}$. These relationships were verified using a fast vacuum photodiode.

Typical output energies with 100mJ of pre-lase Q-switched 1.064 μm radation were ≈ 10mJ at 532nm and 3mJ at 355nm. No attempt was made to maximise these energies by operating with smaller waist-sizes since these energies were more than sufficient to reach threshold in H_2.

4.2 Single-Pass Raman Scattering in Hydrogen

The first experiments performed used SLM pulses at the three wavelengths 1.064μm, 532nm and 355nm which were tightly focussed into the centre of a hydrogen gas filled cell equipped with Brewster windows.

The temporal profiles of the pulses were smooth Gaussians with pulse lengths consistent with the equations of the previous sections. In each case the transmitted pump was monitored with a vacuum photodiode and a transient digitiser, the overall rise time being about 0.5ns. In addition to this, direct detection of the Stokes radiation was performed using a pyroelectric energy meter (Laser Precision Corp. Model RKP 335) and appropriate filtering to eliminate other wavelengths, especially the pump. With 1.064μm as the pump the vacuum photodiode must incorporate an S1 photocathode. This is insensitive to the 1st Stokes at 1.907μm and can be used without filters to monitor pump depletion. The 1.907μm can itself be detected and measured using the pyroelectric energy meter and a germanium filter. This blocks all radiation with a wavelength shorter than 1.8μm. It transmits about 30% at 1.907μm. With 532nm or 355nm radiation as the pump the 1st Stokes wavelengths are at 683nm and 416nm respectively. Both an S1 and an S20 photo-cathode will respond well to all four of these wavelengths, and so some filtering is necessary. Perhaps the best way is to use a prism and then some aperture to separate off the required component, and this was the method used here.

For each of the three pump wavelengths the Raman threshold was measured at a hydrogen pressure of ~435 psi (~30 Atm) which is well into the pressure broadened regime and hence gives the minimum threshold. Threshold was measured by varying the transmission of the two-plate attenuator until either (i) the smooth temporal profile of the transmitted pump had a tiny notch taken out of it near the peak, or (ii) the pyroelectric energy meter just detected 1st Stokes on every shot (This corresponded to an energy of about 1μJ).

The pump threshold power was obtained by measuring the pulse energy just before the cell, measuring the pulse length (FWHM) and substituting them into the equation;

$$P_{p,th} = \frac{0.94 \times E(thresh)}{\tau(FWHM)} \qquad 4.3$$

Where the factor 0.94 is a consequence of treating the time behaviour as having a Gaussian shape.

The experimental results are presented in the table below alongside the theoretically predicted results of the last chapter. As can be seen there is agreement to within 10%. This suggests that our estimate of the errors in the theoretical values are a little pessimistic.

Table 4.1 Experimental and Theoretical Thresholds for Unguided SRS in H_2

Pump wavelength (nm)	1064	532	355
1st Stokes wavelength (nm)	1904	683	416
Focussing: L/b_p	9	3	13
Theoretical threshold (kW)	1370	175	50
Experimental threshold (kW)	1340	155	50

A more searching test of the theory involved the case of 1.064μm pump pulses of various linewidths in hydrogen at various pressures. Multi-mode, single mode and two-mode pulses were used and the pressure was varied between ~8Atm and 35 Atm. This experiment is described more fully in Berry and Hanna(1983) which is reproduced in appendix II. The graph of the results is also presented here as fig. 4.5. As can be seen, the experimental values for multi-mode and single-mode pulses are in excellent agreement with the theory curve taken from chapter 3. The two-mode thresholds are lower as predicted, although they do not decrease by the factor of two that would have been expected if the medium showed a steady-state response even to the modulated structure of the pump pulse. A more careful consideration of the nonlinear growth of the Stokes wave (Ibison, 1982) suggests that only at much higher pressures would the steady-state response be fully achieved.

It is clear from these results that we have at our disposal a good understanding, and usuable theory, of stimulated Raman scattering in hydrogen. For methane the occurrence of SBS under conditions of single-pass pumping and single mode operation precluded a study of SRS as achieved for H_2. However, experimental results for SRS in methane obtained under different circumstances indicate also a good agreement with theory. We will go on in the next section to describe experiments which test the theoretical predictions for SBS.

4.3 Single Pass Raman and Brillouin Scattering in Methane

Experiments were performed to investigate the response of methane gas at various pressures to tightly focussed, SLM and multimode, 1.064μm pump pulses of about 30ns duration.

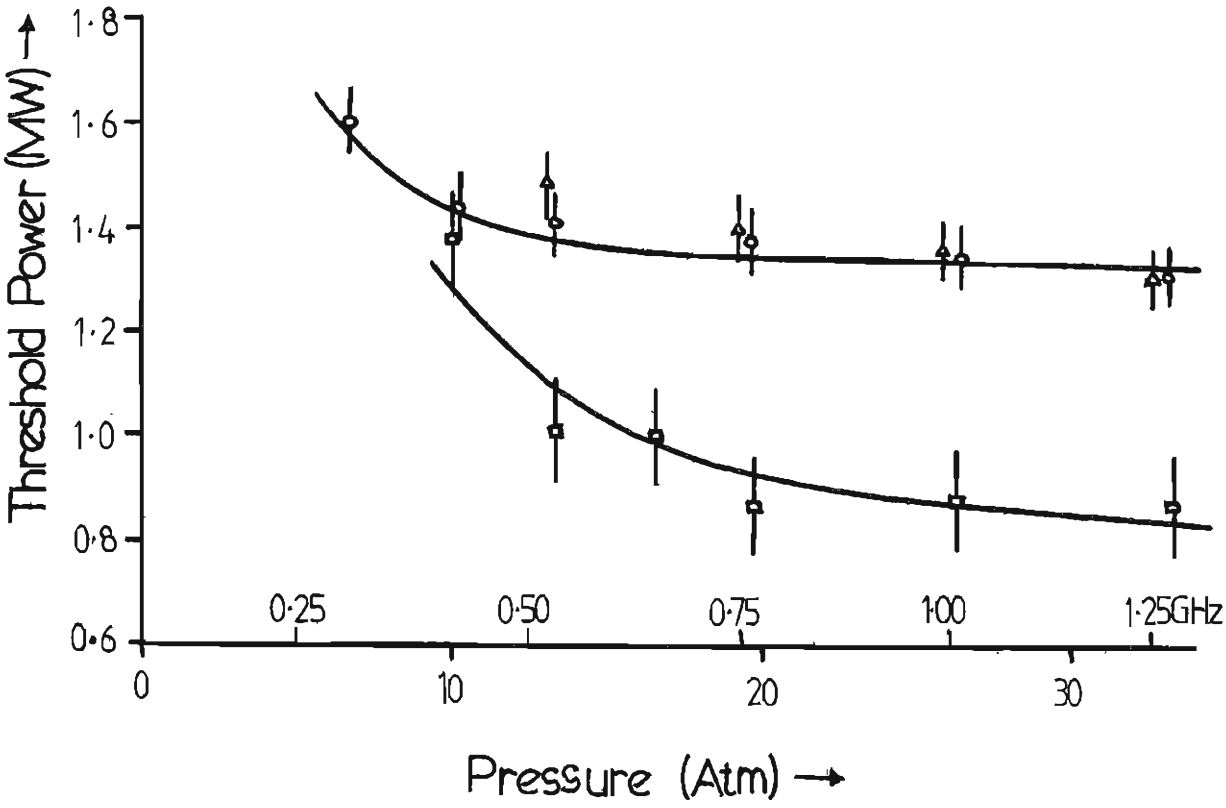

Figure 4.5: Stimulated vibrational Raman threshold power for a 1.064μm pump in hydrogen gas as a function of gas pressure. Linewidth (FWHM) of the Raman transition in GHz is also indicated. The upper solid curve is a theoretical calculation taken from the equations of chapter 3. Experimental points correspond to; o - SLM pump, □ - two-mode pump, Δ - multimode pump.

The basic experimental arrangement is again as shown in fig. 4.1. Any Brillouin scattered radiation will occur in the backwards direction and so some explanation of the diagnostics is necessary. It is also necessary at this point to consider the polarisation of the pump beam and how the threshold depends on it. Hitherto, linearly polarised light has been assumed in the theory of chapter 3 and used experimentally so far in this chapter. Now Brillouin scattered radiation, travelling in the backwards direction (and also the phase conjugate of the pump beam) would re-enter the laser cavity and thereby alter its performance, and also that of the Brillouin scattering process itself. To prevent this effect the laser and Brillouin cell can be isolated either by making the distance between them very large (i.e. with a transit time greater than half the pulse width); by using a $\lambda/4$-plate and polariser as shown in the box in fig. 4.1, or by using the well known Faraday rotator and polariser technique. Faraday rotators are bulky and expensive, although they do result in the presentation of linearly polarised light to the Brillouin cell. The $\lambda/4$-plate and polariser combination is much more convenient and compact and needs no bulky power supply. The only disadvantage is that it presents circularly polarised light to the Brillouin cell. Fortunately, however, the experimentally measured Brillouin scattering thresholds for circularly polarised light are the same as those for linearly polarised light to within experimental error. The main disadvantage, therefore, that the $\lambda/4$-plate has over the Faraday rotator is that a Brewster input window cannot now be used on the Brillouin cell.

When measuring Brillouin Scattering thresholds with circularly polarised pump radiation threshold could be detected either by monitoring the transmitted pump and looking for slight depletion (not possible for multimode pump pulses) or by detecting the Brillouin scattered radiation at 1.064μm being rejected by the polariser.

This could be done with either a pyroelectric energy meter for quantitative measurements above threshold, or a phosphor card for just threshold detection. When using linearly polarised light straight from the laser, threshold could again be detected by monitoring the pump, by monitoring the reflection off an angled glass plate through which the input beam is passed, or alternatively, by detecting the appearance of a small subsidiary pulse delayed from the peak of the main transmitted pulse by the laser to Brillouin cell round-trip time.

Raman Scattering thresholds were detected in the same way as for hydrogen. The Raman shift in methane is $2916cm^{-1}$ resulting in a 1st Stokes wavelength of 1.544μm. Thus, a silicon filter can be used to discriminate between pump and 1st Stokes, a Judson J12 or pyroelectric energy meter performing the detection. Alternatively, 2nd antistokes at 656.6nm can be visually detected.

The experimental results, using focussing conditions of $\tan^{-1}(L/b_p) = 1.31$ in a cell 44cm long, are presented in table 4.2 below and also on the graph of fig. 4.6. Results were taken using linearly polarised SLM and multimode pulses, and also circularly polarised SLM pulses, as the methane pressure was varied between 250 and 500 psi. In all cases the pulse lengths were ~30ns. For the circularly polarised case the energy in the Brillouin Scattered beam was also measured, allowing the reflectivity of the Brillouin cell to be determined. This is simply the ratio of the energy in the Brillouin Scattered beam to that in the input pump beam. Thus, a fixed pump energy of 37.75mJ was input at each methane pressure allowing the variation of reflectivity with pressure to be demonstrated.

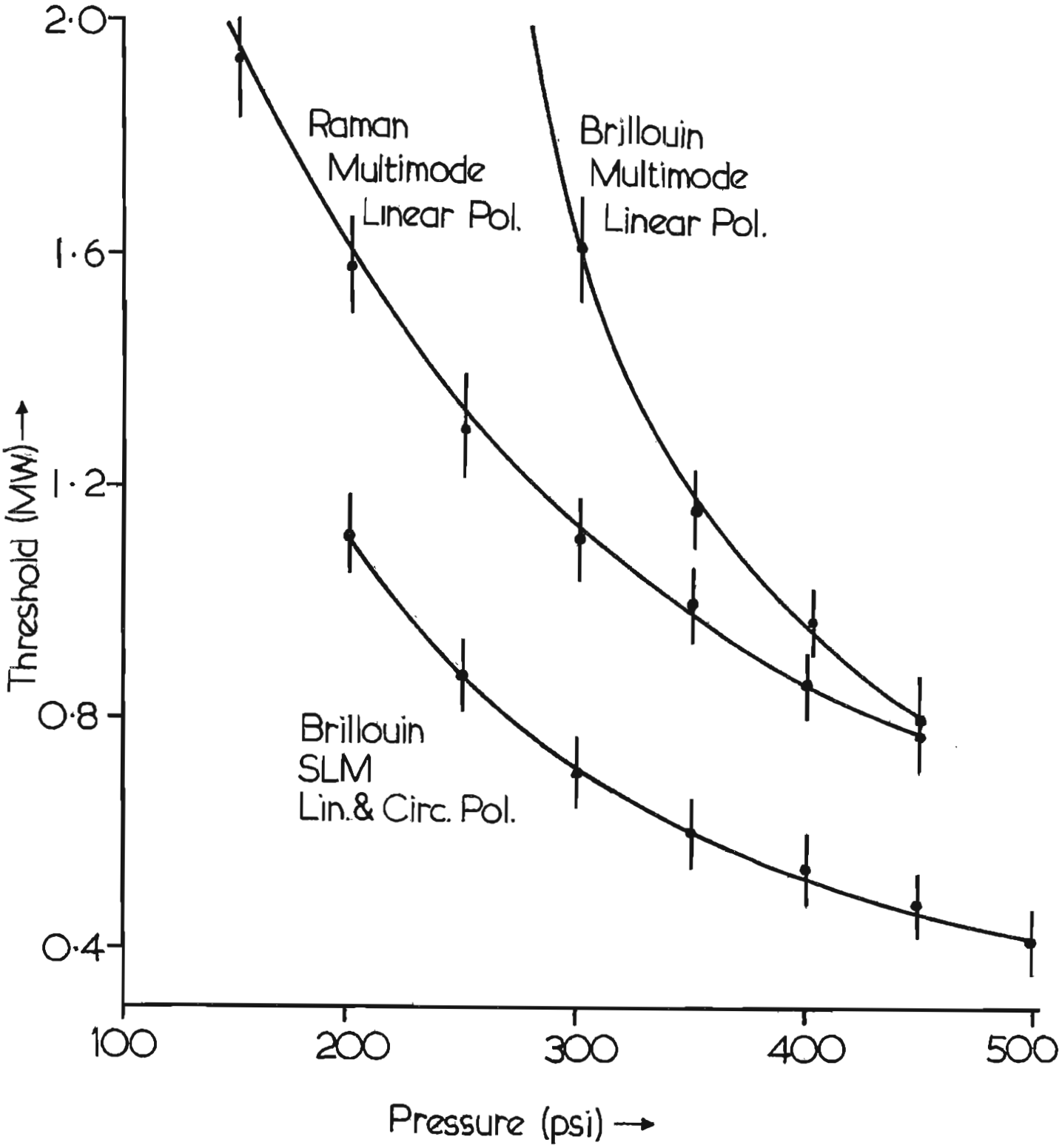

Figure 4.6: Raman and Brillouin thresholds in methane gas at various pressures.

In the case of the linearly polarised, multimode pump Raman scattering threshold was reached before Brillouin scattering started for all but the highest pressures. For these measurements, therefore, the pump power was increased above Raman threshold until Brillouin scattering was also detected. Brillouin threshold was therefore also measured.

Table 4.2 Unguided, tight-focussing SRS and SBS thresholds for 1.064μm Pumping in CH_4

Pressure (psi)	Raman Th.(MW) multi,linear	Brill.Th.(MW) multi,linear	Brill.Th.(MW) S.L.M,linear	Brill.Th.(MW) S.L.M, circular	Reflectivity (%) S.L.M, circular
150	1.93				
200	1.57		1.11	1.18	0
250	1.29		0.87	0.845	9.5
300	1.11	1.61	0.70	0.74	19
350	1.00	1.15	0.60		
400	0.86	0.97	0.54	0.42	32
450	0.77	0.79	0.48		
500	0.70	0.70	0.42	0.32	35

As can be seen the linearly and circularly polarised SLM results are approximately the same at all the pressures measured. Also, Raman scattering does not occur, as expected, for these pulses due, of course, to the fact that the Brillouin gain is always higher.

Even if the pump intensity were increased way above Brillouin threshold the Brillouin effect would deplete the pump and thereby still prevent Raman threshold being reached. The Brillouin thresholds are higher for multimode pulses than for single mode pulses, probably as a result of two combined effects. Firstly, for forward Raman scattering, the increased threshold that would result from the transient character of the pump fluctuations is offset by the fact that a Stokes wave can travel with the high intensity fluctuation. For backwards SRS and SBS the Stokes wave cannot avail itself of the peak intensity over the entire interaction length. Secondly, Raman threshold is reached first as a result of this, the pump pulse is depleted by SRS and the Brillouin threshold is made even higher. The multimode Raman thresholds are much lower than those predicted in chapter 3 for the steady-state for the reasons outlined in section 3.3 of that chapter. Namely, the Raman response time of the medium is so fast that it is comparable to the typical durations of the fluctuations within the multimode pulses. Since these fluctuations have powers much higher than the average powers of table 4.2 and fig. 4.6, and yet are still nearly steady-state, Raman threshold is reached.

But how do the single-mode Brillouin thresholds measured compare with those predicted from the theory of chapter 3? Fig. 4.7 shows a graph of our experimental results as compared with the theoretical values from table 3.4. Three theoretical curves are plotted (i) the steady-state theory using the focussing analysis of Cotter et al embodied in equation 3.25; (ii) the transient theory using Cotter's analysis and (iii) the transient theory using Trutna and Byer's treatment of focussed beams embodied in equation 3.60.

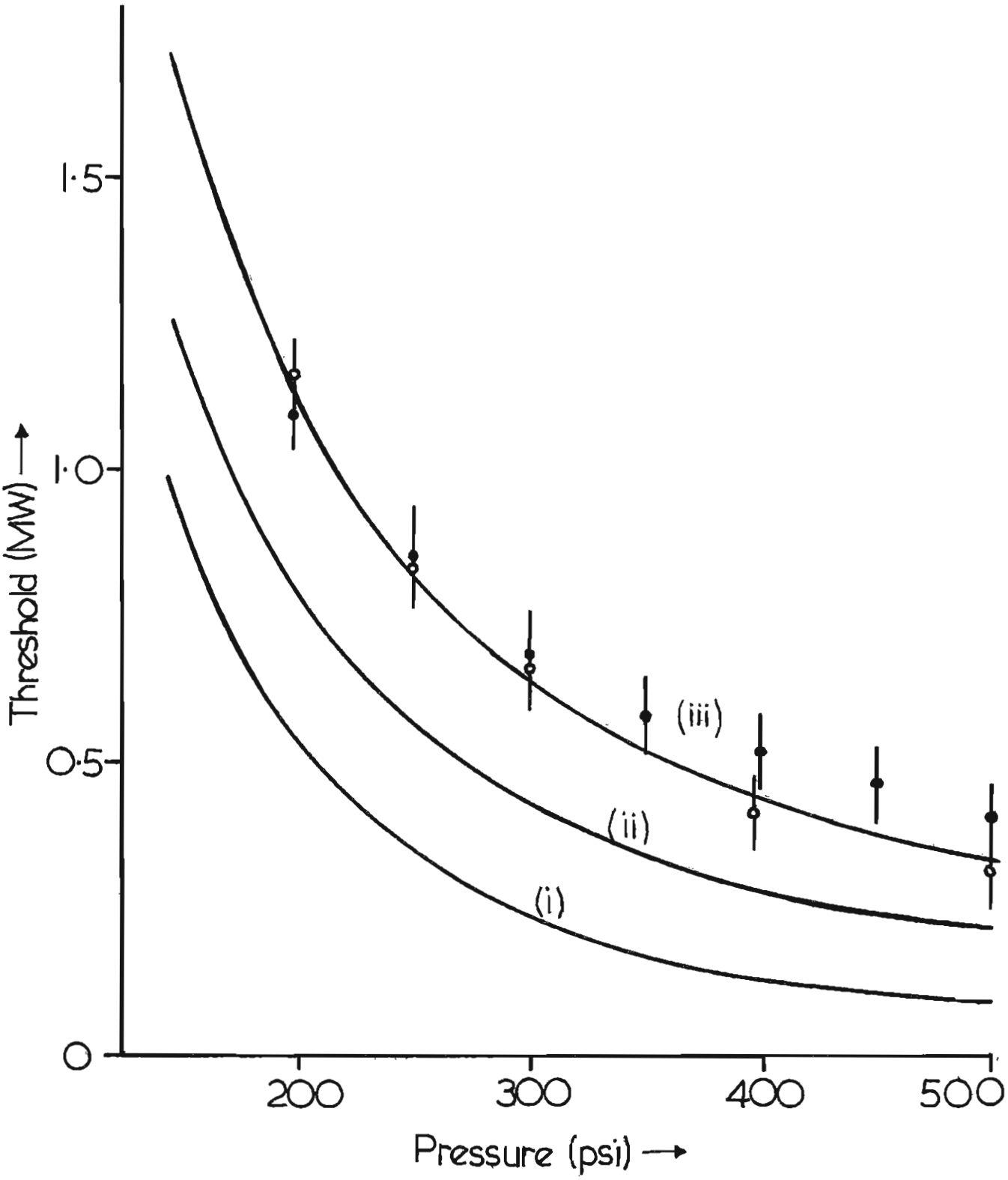

Figure 4.7: Comparison between experimental and theoretical Brillouin thresholds. • - linear polarisation, o - circular pol.

As expected, the transient theory curves are much closer to the experimental results. Not only this, however, the transient theory of Trutna and Byer coincides almost exactly with the experimental results whereas hitherto Cotter's focussing theory has been applied with remarkable success. In fact, however, the possible errors in the theoretical threshold calculations are likely to be worse than the ~30% estimated earlier for SRS.

We have here additional uncertainties connected with the transient analysis, the derivation of $[\rho \partial\epsilon/\partial\rho]$ and also the phonon lifetimes. Errors as large as a factor of 2 are therefore not unlikely and so the results of fig. 4.7 cannot be considered to give a definite demonstration of the validity of Trutna and Byer's theory.

Either way, it seems as though we have an adequate understanding of Brillouin scattering theory to make useful predictions from it. The main use of this theory, as we shall see, is to be able to predict when the Raman gain is higher than the Brillouin gain, thereby allowing us to generate wavelengths further into the infrared.

4.4 Raman Scattering in a Hydrogen Raman Oscillator

The oscillator theory of section 3.6 of the last chapter was checked briefly for the case of Raman Scattering in hydrogen. Although many similar experiments have been reported elsewhere (e.g. Avizonis and Heimlich, 1959 or McClung and Close, 1969) none have used quite the same analysis as section 3.6 nor had as well defined a pump pulse as provided by the pre-lase Q-switched telescopic resonator.

The experimental arrangement is shown in fig.4.8. For various reasons it was difficult to satisfy the minimum threshold requirement of $(W_{S0}/W_{P0}) = (\lambda s/\lambda p)^{\frac{1}{2}}$ obtained from equation 3.65, and so a typical experiment had the following parameters. The gas cell was filled to 350 psi with hydrogen and consisted of a gain medium of length $L_g = 32$cm between Brewster windows. Lenses 1 and 2 were both uncoated and had focal lengths of 30cm. Mirror 1 had a reflectivity at 1.907μm of ~100%, and so when combined with the uncoated lens gave a net reflectivity of $R_1 = 0.84$. Similarly mirror2 was 39% reflective at 1.907μm giving $R_2 = 0.23$. The lenses were placed fairly close to the mirrors and resulted in a cavity of overall length $L_C = 65.5$ cm (when the distance between the lenses was 57cm). Equation 3.63 predicts a Stokes spotsize at the centre of the resonator of 199μm. Using a 1m matching lens, and lengths $l_1 = 189.5$cm, $l_2 = 44$cm, a pump waist size of 68μm occurs at the centre of the resonator. The pump pulse length on this occasion was 36ns. When using equation 3.68 to predict the threshold power one must be careful not to confuse the gain medium length with the cavity length. The latter must be used to calculate the cavity transit time, whereas the former must be used in the $\tan^{-1}(LB/2)$ term. Including all these values in equation 3.68 gives a theoretical threshold peak pump power of $P_p = 340$kW, with threshold reached after 21 cavity transits. This should result in a notch being taken out of the transmitted pump profile ~21ns after the peak. Experimentally the threshold was measured by varying the transmission of the beam attenuator until just such a notch appeared (fig.4.9). Its position is, indeed, ~20ns after the peak. The measured threshold was (using equation 4.3), $P_p(\text{exp}) = 385$kW which represents a 13% error on the theoretical result, well within expected possible errors. It would appear, therefore, that we have an adequate theory for dealing with unguided resonator configurations.

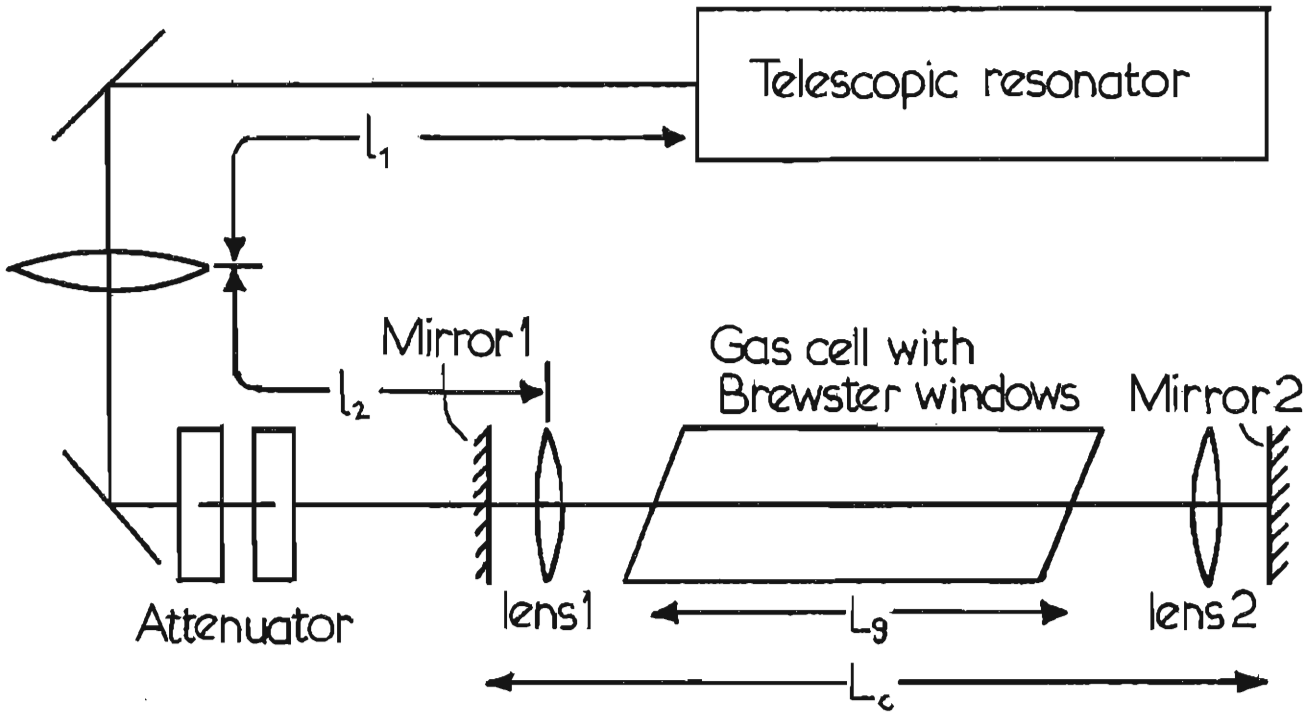

Figure 4.8: Basic Raman oscillator experiment.

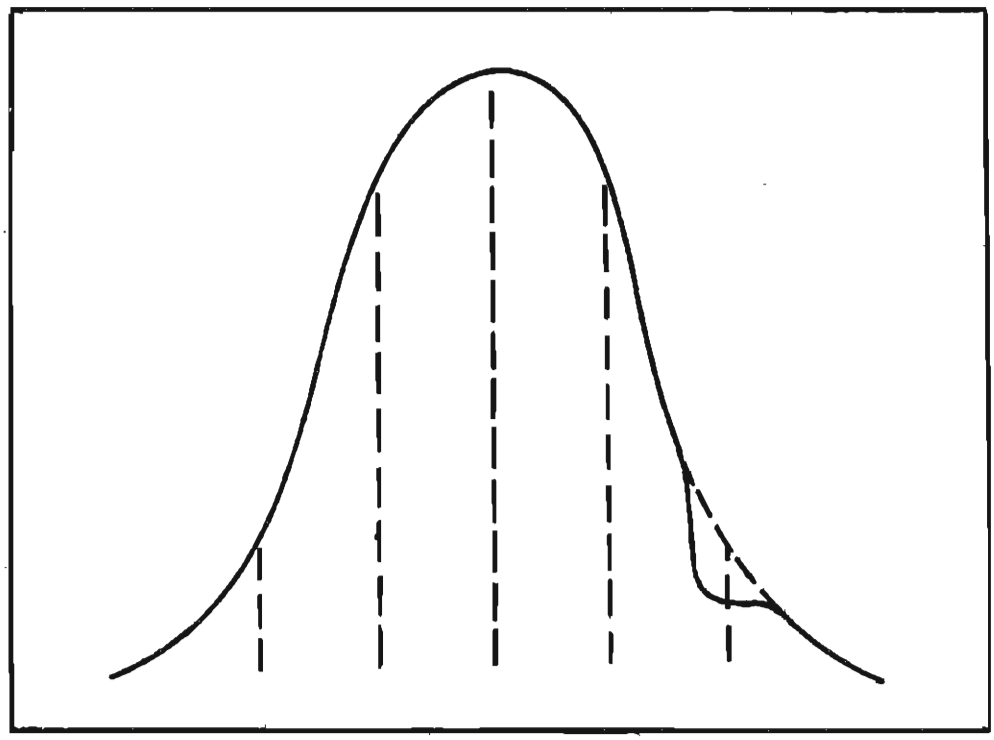

Figure 4.9: Transmitted pump profile just on threshold. (10ns/div)